Transmission mode impacts parasite spread in spatially structured environments

Franziska A. Brenninger[1*] and Xiang-Yi Li Richter[1,2]

[1*]Institute of Ecology and Evolution, University of Bern, Baltzerstrasse 6 , 3012, Bern, Switzerland.
[2]Department of Biology, University of Konstanz, Universitätsstraße 10, 78464, Konstanz, Germany.

*Corresponding author(s). E-mail(s): f.brenninger.evobio@outlook.com;

Keywords: transmission mode, parasite, vertical transmission, horizontal transmission, mixed-mode transmission, dispersal, spatial structure, infection spread

Author Contributions Conceptualization: F.A.B. and X.Y.L.R.; Creation of the model: F.A.B. and X.Y.L.R.; Analyses of results: F.A.B.; writing of first draft: F.A.B.; revision and editing of the manuscript: F.A.B. and X.Y.L.R.

Data accessibility statement The code to produce the results and figures can be made available upon request and will be made publicly available following peer-reviewed publication in zenodo DOI:10.5281/zenodo.21279859.

Running Title Transmission modes and spatial structure

Type of Article Letter

Words in the Abstract 149

Words in the Text 4319; (excl. abstract, acknowledgments, references, table and

figure legends)

Number of References 66

Number of Figures, Tables, Text boxes in the main text 5,1,0

Abstract

The spread of parasites and pathogens is shaped by their transmission to new hosts and often inherently linked to the spatial structure of host populations. Transmission modes are typically classified as either horizontal — between individuals — or vertical, from parent to offspring. While some parasites rely exclusively on one mode, many use both. We investigate how transmission mode impacts the spread of a parasite in different spatially structured metapopulations with variable habitat size and host dispersal propensity depending on infection status. We find that patch size disparities together with infection dependent dispersal result in local infection prevalence that deviates from single patch expectations, whereby the nature of this deviation differs depending on transmission mode. This work systematically shows how parasite transmission mode alters infection spread through spatially structured environments and highlights that transmission modes can have distinct impacts on the evolution of host-parasite dynamics with potential consequences for disease management.

1 Introduction

Parasite transmission is an essential part of host-parasite dynamics, as parasites balance the exploitation of the current host with transmission to the next to achieve optimal lifetime fitness (Anderson and May 1982; Ewald 1983; Massad 1987). Similar to virulence, transmission of a parasite is the result of combining multiple parasite and host traits, such as the parasite's ability to infect and establish in a new host and the host's immune defense (Antonovics et al. 2017). In general, transmission mode is broadly categorized as either vertical, meaning the parasite transmits from parent to offspring, or horizontal, where parasites transmit from one host to the next, independent of relatedness. While some parasites predominantly use one transmission mode (e.g., vertically transmitted endosymbionts in arthropods (Hurst and Frost 2015); horizontal transmission of measles (Getahun et al. 2017) or rabies virus (Hankins and Rosekrans 2004)), others spread through a mix of modes (see (Ebert 2013) for a review), and for many, the full range of transmission pathways remain yet to be identified (Antonovics 2017).

The overarching categories of transmission mode can be further subdivided to specify the nature of parasite transmission in more detail (Antonovics et al. 2017). For instance, vector-borne, airborne, or environmentally transmitted diseases all transmit horizontally, but follow different dynamics when transmitting to a new host. Horizontal transmission of pathogens that spread via vector species, like Malaria or Dengue virus (Meibalan and Marti 2017; Cattarino et al. 2020), or parasites that are passed through sexual contact between hosts, such as Chlamydia or Gonorrhea (Da Ros and da Silva Schmitt 2008), are often modeled as frequency dependent. The underlying assumption is that each infected individual makes a constant number of potentially infectious contacts per unit time, for example, the number of sexual contacts in a population or the biting rate of a mosquito. Then, the chance of becoming infected primarily depends on the frequency of infected individuals in a population. The spread of other horizontally transmitted parasites is better described by density-dependent (mass-action) transmission. This applies whenever contact rates between

individuals change with host density, as is the case in airborne diseases, when released droplets or aerosols can infect more hosts the more host individuals are present (McCallum et al. 2001; Begon et al. 2002; Thrall et al. 1993).

Transmission of a parasite is inherently linked with spatial structure, as host populations tend to be distributed across different habitats and parasites need to move directly or indirectly to encounter susceptible hosts. Incorporating space into host-parasite dynamics yields key insights into epidemiology and parasite ecology (Riley 2007; Guégan et al. 2005). For instance, metapopulation models have shown that connectivity between patches shapes local oscillatory infection dynamics (Xia et al. 2004). Similarly, specific levels of dispersal in a metapopulation can maintain infections that would not persist in a single well-mixed population (Hagenaars et al. 2004) or limit infection to isolated subpopulations (Post et al. 1983). The most tractable metapopulation framework is a two-patch model, in which dispersal connects patches that may differ in size (as in mainland–island systems). Two-patch models have been applied widely to examine how various ecological processes play out in a spatially structured environment (Grumbach et al. 2023; Szilágyi and Meszéna 2009; Cressman and Křivan 2013; Acevedo et al. 2015). Extending these two patch models to randomly generated networks of multiple interconnected patches allows for increased realism while maintaining interpretability of the core dynamics. For instance, randomly generated networks have been used to estimate epidemiological disease waves (Lang et al. 2018; Lloyd and Jansen 2004) and population persistence in fragmented landscapes (Grilli et al. 2015). Such network models can provide a baseline for understanding dynamics arising in metapopulation models that add more biological complications, such as locally variable infection rates (Acevedo et al. 2015) or stage specific extinction risks (Sutherland et al. 2014).

It is well established that transmission mode is a key determinant of parasite spread and persistence within a single patch (Lipsitch et al. 1995, 1996). However, existing spatially structured models typically focus on a single transmission mode

inspired by a host–parasite pairing of interest (Lloyd and Sattenspiel 2009; Fulford et al. 2002; Hickson et al. 2012; Gaff and Gross 2007; Zeng et al. 2023), which limits general insights across systems. The few cases examining parasites with multiple transmission modes, usually involving at most two, demonstrate that transmission can strongly shape spatial patterns of infection (Shaw et al. 2019; Fulford et al. 2002; Berngruber et al. 2015; Ryder et al. 2007).
Thus, a priori expectations of whether and to what extent different transmission modes shape parasite spread across space remains unexplored.

Here, we adopt a systematic approach to examine how commonly considered parasite transmission modes — frequency-dependent horizontal transmission, density-dependent horizontal transmission, vertical transmission, and corresponding mixed-mode transmissions — interact with spatial structure to shape parasite spread and prevalence. Extending classical SIS (susceptible-infected-susceptible) frameworks, we develop spatially explicit UIU (uninfected–infected–uninfected) models. Here, we adapt the terminology to account for the fact that, under exclusive vertical transmission, uninfected individuals are per definition never 'susceptible'. To establish baseline expectations for how transmission mode, host dispersal and spatial structure influence infection spread, we analyze parasite dynamics across one-patch, two-patch, and randomly generated network scenarios. This study aims to advance fundamental understanding in spatial epidemiology and inform future theoretical and empirical work on parasite invasion and disease dynamics, which also highlights the importance of transmission mode for host-parasite dynamics and its potential for evolutionary adaptation.

2 Material and methods

To investigate how transmission mode of a parasite influences infection dynamics in space, we adapt several UIU models to compare a total of five different transmission modes: (1) frequency-dependent horizontal transmission (FD), (2) density-dependent

horizontal transmission (DD), (3) vertical transmission (V), (4) mixed-mode transmission with frequency-dependent horizontal and vertical transmission (FD+V) and (5) mixed-mode transmission with density-dependent horizontal and vertical transmission (DD+V) (figure 1). In the following, we derive the infection dynamics for a parasite using mixed-mode transmission, as this includes all components of the individual transmission modes. The detailed derivations for each individual transmission mode are provided in Supplementary Information S1. We first detail the dynamics within a single isolated patch, before adding spatial structure to our model later.

2.1 Single patch dynamics

We assume a well-mixed, asexually reproducing population of uninfected and infected individuals, denoted by U and I, respectively. Total population size N is calculated as $N = U + I$. We can describe the infection dynamics in a population infected with a parasite that can transmit both horizontally and vertically as

$$\begin{aligned} \frac{dU}{dt} &= \alpha_U U + \alpha_I(1-\beta_v)I + \mu I - \Omega - d_U U - \theta N U, \\ \frac{dI}{dt} &= \alpha_I \beta_v I + \Omega - \mu I - d_I I - \theta N I. \end{aligned} \tag{1}$$

Here, α is the per capita growth rate and d the baseline mortality for uninfected and infected individuals, as indicated by the subscript $_U$ and $_I$, respectively. We assume that both fertility and mortality can differ with infection state, as infected individuals may experience higher mortality and reduced fertility compared to healthy conspecifics. The population is subject to density-dependent mortality, where increased crowding in the environment results in higher mortality. This effect is scaled by the parameter θ, modulating the strength of density-dependent mortality.

Individuals can inherit the parasite (vertical transmission) or get infected during their life (horizontal transmission). Vertical transmission efficiency is denoted by β_v, representing the proportion of offspring that inherit the parasite from an infected parent. The remaining proportion $1 - \beta_v$ consists of offspring that did not inherit the parasite due to vertical transmission failure and is instead added to the number of

uninfected individuals in the population. Horizontal transmission is captured by infection rate Ω. In cases where horizontal transmission is frequency dependent, Ω takes the form of $c\beta_h \frac{I}{N} U$, where c is the encounter rate between individuals. The probability of encountering an infected individual is given by the frequency of infected individuals in the population, $\frac{I}{N}$, and upon contact, horizontal transmission of the parasite occurs with horizontal transmission efficiency β_h. When horizontal transmission is density-dependent, Ω takes the form of $c\beta_h IU$. In this case, the transmission of infection increases as population density grows (density-dependent or mass-action infection). Thus, the rate of new infections is proportional to the number of infected and uninfected individuals in the population IU and scaled by the contact rate and transmission efficiency of the parasite $c\beta_h$. Infected individuals can recover and lose the infection at rate μ. See figure 1 for a flow diagram corresponding to equations 1 and table 1 for a list of all symbols.

2.2 Dynamics with spatial structure

To determine how infection dynamics can differ in a spatially structured system, we consider a set of distinct habitats — also referred to as patches — connected by the dispersal of individuals between them. The dynamics of such a system are then the combined result of local infection spread and dispersal between patches, which we describe following Jansen and Lloyd 2000 with

$$\hat{x}_j = f(x_j) + \sum_{i=1}^{n} s_{ij} \boldsymbol{M} x_i. \tag{2}$$

Here, x_j denotes a vector containing the densities of the different types of individuals (U, I) within patch j, with $f(x_j)$ accounting for the local dynamics. Local dynamics are defined depending on the transmission mode (see equations 1, S1, S4, S8, S11, S14). The diagonal migration matrix $\boldsymbol{M}$ denotes dispersal propensity for the different types of individuals, while the connections between the patches is described by the connectivity matrix $\boldsymbol{S}$. Hereby, we assume that infected and uninfected individuals can reach the same habitats, but the proportion of individuals that disperse can differ depending on infection state. Infected individuals, for example, may become more or less likely to

move to a new patch compared to uninfected con-specifics (Bradley and Altizer 2005; Debeffe et al. 2014; Brophy and Luong 2022). Thus, we define two different dispersal propensities m_U and m_I, referring to uninfected and infected individuals, respectively. Individuals cannot get infected or recover during dispersal, meaning that infection status can only change within a patch.

2.2.1 Mainland-island model

First, we consider a case with two habitats of different sizes that are connected by dispersing individuals. The size difference between the two habitats is determined by the patch specific density-dependent mortality θ_i, θ_j. A larger density-dependent mortality θ, corresponds to a smaller habitat, where individual mortality increases at comparatively lower levels of crowding. Note that this form of population size regulation does not impose a strict carrying capacity. See Supplementary Information S2 and equations therein for concrete examples of implementation of two-patch dynamics for each transmission mode.

2.2.2 Randomly generated networks

We next extend our analysis by simulating the effects of different transmission modes within more complex spatial structures by considering a network of multiple patches generated by a random geometric graph. To generate the network, we assign a location to each patch, by randomly picking x- and y- coordinates between 0 and 1 following a uniform distribution. Patch connections are determined by the network connectedness parameter a, defining the maximum distances within which patches remain connected. If the distance between patch i and j is smaller or equal to a, the two habitats are connected, otherwise habitats are too distant from each other to allow successful dispersal.

Table 1 Symbols and meanings.

Symbol	Meaning
U	Number of uninfected individuals in the population
I	Number of infected individuals in the population
N	Total population size calculated by $N = U + I$
α_U	Per capita growth rate of uninfected individuals
α_I	Per capita growth rate of infected individuals
β_h	Horizontal transmission efficiency
β_v	Vertical transmission efficiency
c	Contact rate
d_U	Baseline mortality of uninfected individuals
d_I	Baseline mortality of infected individuals
θ	Strength of population density regulation
μ	Recovery rate from infection
Subscripts i, j	Subscripts i and j refer to two different patches
x_j	Vector containing the densities of the different types of individuals (U, I) in patch j
$\boldsymbol{M}$	Migration matrix containing dispersal probabilities
m_U, m_I	Dispersal probability for uninfected and infected individuals, respectively
$\boldsymbol{S}$	Connectivity matrix describing spatial structure of the different patches
$s_{i,j}$	Element of the connectivity matrix describing the connection from patch i to j
a	Network connectedness in a geometric network graph describing the maximum distance at which two patches can be connected

3 Results

Quantitative comparisons between the different transmission modes are inherently challenging, as each mode is characterized with somewhat distinct parameters. Further, the effect of a parameter can scale differently within each mode. At low values of $c < 0.1$, for example, frequency-dependent transmission can fail to produce sustained infection spread, whereas the same values may suffice when transmission is density-dependent. To account for such disparities and avoid instant fixation of, for example, density-dependent infection, we chose different c values for the two horizontal transmission modes in the results below. While this precludes direct quantitative

comparison between the different transmission modes, we here focus on a qualitative comparison with the aim to understand the interaction between infection dynamics of parasites using different transmission modes across different spatial structures.

3.1 Single patch dynamics

Within a single patch, distinct infection dynamics arise from the different transmission modes. The main difference between the two horizontal transmission modes is whether transmission can be amplified by higher population density (density-dependence) or higher infection frequency (frequency-dependence). A parasite that is transmitted solely horizontally in a frequency dependent manner, would reduce its own transmission when conferring a fecundity benefit to infected hosts, because infected individuals only produce uninfected offspring. With increased birth of uninfected offspring the infection frequency in the population lowers, which results in less infection transmission (following $c\beta_h \frac{I}{N} U$) (figure 2a). In contrast, higher host fecundity with a density-dependent horizontally transmitting parasite can speed up transmission as individuals accumulate faster in the patch. Regardless, the parasite will reach the same equilibrium frequency independent of host fecundity, as long as maximum patch population size remains stable (figure 2b). While horizontally transmitted parasites can spread even when infection imposes a fecundity costs on the host (e.g., $\alpha_I < 1$, when $\alpha_U = 1$), provided that transmission efficiency (β_h) and contact rate (c) are sufficiently high — vertically transmitted parasites require high transmission efficiency β_v and/or a fecundity advantage in infected hosts (e.g., $\alpha_I > 1$, when $\alpha_U = 1$) to spread in a population (figure 2c).

These insights extend to mixed-mode transmission (figure 2d,e). When mixed-mode includes frequency-dependent horizontal transmission (FD+V), the benefits that increased fecundity in infected individuals brings to vertical transmission weigh against the reduction in transmission for FD horizontal transmission, such that the equilibrium infection prevalence varies depending on which transmission pathway is used more (figure 2d). When transmission is density-dependent horizontal and vertical (DD+V), a fecundity boost in infected hosts ($\alpha_I > \alpha_U$) generally increases

the equilibrium infection frequency in a patch (figure 2e).

In the mixed-mode transmission cases, the proportion of new infections arising from horizontal or vertical transmission changes with increasing infection prevalence in the population (figure S8). When horizontal transmission is density dependent (DD+V), the proportion of infections gained via horizontal transmission at low population size is small and increases with population size. For frequency-dependent transmission, the proportion of horizontally gained new infections remains stable regardless of population size increase. For both cases, the proportion of new infections acquired by horizontal transmission eventually declines as the parasite becomes widespread in the population and most infections are gained via the vertical transmission pathway (figure S8).

3.2 Spatial structure

3.2.1 Mainland-island model

In the mainland-island scenario, infection prevalence converges on the same single-patch equilibrium in both patches when the patches are of equal size, because the number of individuals leaving a patch matches the number of individuals arriving irrespective of the dispersal propensity (figure S9a-e). When the two patches differ in size, the number of dispersers arriving no longer equals the number of dispersers leaving. Differences in dispersal propensity between infected and uninfected individuals can then alter the infection prevalence in both patches. Generally, the type of individual (infected or uninfected) that disperses more tends to accumulate in higher numbers in the smaller patch, shifting the local prevalence toward the more dispersive type. In the larger patch, more of the dispersive individuals leave the patch than enter from the smaller patch, which biases the composition there toward individuals that are more likely to stay. For example, when infected individuals disperse more readily than uninfected ones, infection prevalence tends to be higher in the smaller patch, while the infection prevalence in the larger patch is comparatively reduced. When dispersal rates do not vary with infection status, the system converges on the

same infection prevalence in both patches (figure 3a,d; white diagonal line).

Deviations from this pattern occur under specific parameter combinations for some of the transmission modes. In the case of density-dependent horizontal transmission, higher population density of the larger patch leads to increased transmission compared to the smaller patch. This amplified transmission rate in the larger patch can partially offset net migration losses (individuals arriving<individuals leaving) of infected individuals, so that under some parameter combinations, the larger patch may still have a higher infection prevalence than the smaller patch, even when infected individuals disperse more than uninfected ones (figure 3b,e; note the shift in the white diagonal line compared to a and d). As the disparity in patch size increases, this effect diminishes, because increasingly negative net migration continuously reduces population density in the larger patch and thus lowers density-dependent transmission (figure 3; shift of the white line from b to e).

In the case of vertical transmission, (infected) individuals arriving in a patch do not impact transmission in the same way as they do under frequency- or density-dependent horizontal transmission. Instead, absolute numbers of immigrants and emigrants play a more direct role in determining infection prevalence, leading to noticeably distinct dynamics when patch size difference increases (figure 3c,f). Importantly, even if individuals of a certain infection status are more likely to disperse, this does not necessarily result in a higher number of dispersers in absolute terms. For instance, if infected individuals have higher dispersal propensity, the larger patch will contain fewer of them due to sustained negative net migration (i.e. the number of infected individuals leaving exceeds the number arriving). In contrast, the dispersal propensity of uninfected individuals is smaller, corresponding to a smaller net migrational loss of uninfected individuals in the larger patch. As a result, the larger habitat equilibrates at low infection prevalence. Then, even if the proportion of infected dispersers is higher than the proportion of uninfected ones, the absolute number of

infected dispersers arriving in a patch can fall below the absolute number of uninfected dispersers arriving, resulting in low infection prevalence in the smaller patch (figure 4a-e). However, when uninfected individuals are very philopatric and barely disperse so that the absolute number of uninfected dispersers remains lower than that of infected dispersers, the smaller patch can reach high infection prevalence even when the larger patch contains predominantly uninfected individuals (figure 3d-h). The same reasoning can explain the patterns emerging when uninfected individuals tend to disperse more than infected ones (figure 4d,e).

3.2.2 Randomly generated network

We extended our analysis to more complex spatial structures and compare how the different transmission modes are impacted by three network types and varying dispersal propensities for infected and uninfected individuals. All three investigated network types have the same number of patches and maximum patch size, but different patch size distributions: one where all patches are the same (maximum) size, one with patches of two different sizes (maximum and ∼55% of the maximum), and one with ten different patch sizes where the size of the patches gradually decreases up to ∼40% of the maximum patch size (figure 5 bottom gray boxes). As network connectedness a expands — and each patch becomes linked to a neighbor — the average global infection prevalence in the network increases across all transmission modes (figure 5, S10, S11). The structural heterogeneity between the replicates results in variation in global infection prevalence at low to intermediate levels of connectedness, when not all patches are connected to the network (figure 5, S10, S11).

At the selected parameter values, the influence of dispersal and network composition on parasites using frequency-dependent transmission is subtle compared to density-dependent and vertical transmission (figure 5). The effects become more discernible when examining the trends at an increased scale (figure 5a,b gray boxes). Because transmission depends on infection frequency within a patch, the proportion

of dispersers joining a patch that are infected or uninfected will, respectively, boost or reduce transmission. Thus, higher infected dispersal can elevate global infection prevalence, whereas increased dispersal of uninfected individuals reduces parasite transmission across the network. This effect strengthens with greater patch size differences in a network, as larger patches contribute more dispersers that disproportionately shift infection frequencies in the smaller recipient patches. Accordingly, dispersal impacts are strongest in the network with two patch sizes, because it has the greatest average patch size difference among the three networks (figure 5a,b). Network connectedness further modulates these dynamics: at intermediate levels of a – all patches are part of the network, but not all patches are universally connected – some patches are relatively isolated and experience net disperser loss, causing local infection frequencies to shift toward the less dispersive types locally. This can counteract the transmission boost or reduction caused by the more dispersive type in well connected parts of the network.

Patch size is the main determinant of global infection prevalence for density-dependent transmission. In the network with gradually decreasing patch sizes, infection prevalence for density-dependent horizontally transmitted parasites is lower compared to the networks composed of two different patch sizes, because the smaller sized patches and therefore reduced local population density constrains transmission and subsequently lowers prevalence. For the same reason, infection prevalence is highest in the same-sized patch network: all patches are the largest size considered in the networks and therefore average density of individuals per patch is the greatest (figure 5 c,d).

Vertically transmitted parasites are most notably impacted by varying dispersal propensity and patch size differences within a network, as increased dispersal of uninfected hosts amplifies global infection prevalence (figure 5f), while greater variation in patch size combined with higher dispersal of infected hosts reduces the resulting global infection prevalence (figure 5e).

In the mixed-mode cases, the effects associated with each horizontal or vertical transmission pathway interact and partially overlap (figure S10). Similar to how transmission mode, network composition and dispersal propensity impact global equilibrium frequencies, they also affect the speed with which parasites reach global infection equilibrium (figure S12).

4 Discussion

Variations to transmission modes, although central to parasite dynamics, have been less of a focal point in epidemiological studies than other parts of host-parasite interactions, such as virulence. Along with recent work increasingly considering multiple and more complex transmission modes, our findings highlight that transmission mode substantially alters parasite spread through space when coupled with varying spatial structure and infection status dependent dispersal. Depending on horizontal transmission mode the number of horizontal transmission events in a patch can change with infection frequency or host density - both factors that are influenced by dispersal propensity, while vertical transmission is naturally linked with the rate of host reproduction. These features have consequences for infection dynamics in space, for example, patch size variation will impact the global equilibrium frequency of density-dependent horizontally transmitted parasites. Higher dispersal of infected individuals slows the spread of parasites using vertical transmission, but will increase transmission in well connected patches for parasites using frequency-dependent horizontal transmission, while decreasing transmission in more isolated patches. Horizontally transmitted parasites can compensate net migratory losses to some extend by enhanced transmission when dispersal leads to locally increased population density or infection frequency. In contrast, vertically transmitted parasites rely more strictly on dispersal numbers to establish in new habitats.

Our findings for the single-patch infection dynamics are consistent with those of (Lipsitch et al. 1995), who examined parasite dynamics when using density-dependent

horizontal, vertical or mixed-mode transmission, in a well-mixed population. We add to the previous results by incorporating frequency-dependent horizontal transmission and adding spatial structure. Vertically transmitted parasites require sufficiently high host fecundity and transmission efficiency to increase in frequency (Ewald 1987; Fine 1984; Lipsitch et al. 1995), making infected host reproduction a non-negligible factor in the dynamics of vertical and mixed-mode transmission. While some parasites can completely castrate hosts upon infection (Baudoin 1975; Lafferty and Kuris 2009) many do not, and an increasing body of evidence suggests that boosting reproductive effort as a response to infection can also act as a form of host tolerance to offset the elevated mortality caused by parasite virulence (Roy and Kirchner 2000; Råberg et al. 2007; Brenninger et al. 2025).

Host–parasite models often consider a horizontally transmitting parasite (Lloyd and Sattenspiel 2009; Hickson et al. 2012; Best et al. 2017; Shaw et al. 2019), but many pathogens can transmit through multiple modes or routes (Antonis et al. 2013; Ebert 2013; Pagán et al. 2014; García-Ordóñez and Pagán 2024). Adding vertical transmission to a horizontal transmission mode (FD+V and DD+V) outperforms the models of each individual transmission mode in terms of increasing infection prevalence and reducing time until global equilibrium, even when parasitic infection comes with a fecundity cost. When a parasite transmits through more than one mode, feedback can arise between the different transmission modes and population composition. Within a single patch, the relative contribution of the different transmission modes shifts as infection prevalence increases: in both mixed-mode scenarios, the proportion of new infections via horizontal transmission declines as susceptible hosts become scarce, and vertical transmission increasingly contributes to new infections (Lipsitch et al. 1995, 1996). Similar dynamics have been reported for mixed-mode transmission in a lattice-structured population model, where a virulent strain initially transmits predominantly through horizontal transmission, but as susceptible hosts become scarce, the strain is mainly transmitted vertically (Berngruber et al. 2015). While we focused on our analyses on combinations of different vertical and horizontal transmission

modes, transmitting via more than one horizontal transmission mode, for example, via sexual and airborne pathways, can also strongly affect parasite dynamics in spatially structured populations. For instance, equipping a predominantly density-dependent transmitting parasite with low levels of frequency-dependent transmission has been shown to enhance infection persistence in spatially structured environments, while adding minor density-dependent transmission to a frequency-dependent transmitting parasite can increase the chances of parasite-driven extinction (Ryder et al. 2007).

Dispersal propensity and patch sizes are critical determinants of infection prevalence in spatially structured populations. Consistent with our findings, a two-patch metapopulation model of horizontal tuberculosis transmission in possums shows that differences in patch carrying capacity increase divergence from single-patch predictions. Larger disparities also dampen infection oscillations, with the smaller patch often exhibiting higher prevalence (Fulford et al. 2002). Empirical results often find that larger patches or patches with high levels of dispersal towards them maintain higher infection prevalence (Laine and Hanski 2006; van Dijk et al. 2022). Our results illustrate the relative importance of infected and uninfected dispersal propensity to shape these patterns and show conditions where the smaller patches can maintain high infection prevalence. Moreover, the tendency for larger patches to contain higher prevalence in natural populations also reflects a lower local extinction risk, which our model does not account for.

We assume an additive benefit for parasites capable of more than one transmission mode in the presented findings. There are empirical examples matching this assumption, for instance, high parasite pressure of the ectoparasite *Ophryocystis elektroscirrha* infecting the American Monarch butterfly (*Danaus plexippus*) enhances transmission via both the horizontal and vertical pathway (De Roode et al. 2009). Contrasting evidence suggests a tradeoff between horizontal and vertical transmission modes in parasites capable of both (Messenger et al. 1999; Turner et al. 1998). In general, transmission mode is variable and can evolve rapidly (Pagán et al. 2014), or be

influenced by a multitude of factors such as competition between different parasites (Harbison et al. 2008; Jones et al. 2011), seasonal variation of host social structures (Smith et al. 2009) or host genotype and environmental conditions (Zilio et al. 2018). Here, our model usefully allows flexible relationships between transmission modes, where tradeoffs are not explicitly imposed, but can be modeled implicitly, depending on parameter settings.

Our findings underscore the importance of considering multiple transmission modes when studying disease dynamics and provide a baseline qualitative expectation for the effects of space and dispersal on parasites that utilize different transmission modes. The current model prioritizes generality and is thus less characterized with system-specific biological details, such as the precise transmission routes parasites can employ and their relative importance in a specific natural population (Cottam et al. 2008). Establishing which transmission modes are utilized in nature is essential, as both horizontal and vertical transmission can distinctly shape infection prevalence and eco-evolutionary feedback between host and parasites. At evolutionary scales, host–parasite dynamics are also likely to be sensitive to differences in transmission mode. In particular, since parasites can act as selective forces on host movement patterns (Pérez-Tris and Bensch 2005; Altizer et al. 2011; Mo 1997; Boulinier et al. 2016; Shaw et al. 2019), different transmission modes may lead to the evolution of distinct dispersal tendencies under otherwise comparable conditions. An outstanding knowledge gap for future work is thus whether and to what extend different transmission modes influence the the evolution of host movement patterns.

Disentangling effects of transmission mode on host spread provides a baseline for interpreting more complex ecological and evolutionary scenarios and making more informed predictions on the evolution of transmission mode. From an applied perspective, interventions that reduce transmission are often used to manage disease spread and virulence, but their efficacy depends on comprehending the underlying evolutionary potential of transmission mode and its impact on infection dynamics in spatially

structured networks. By clarifying how transmission strategy and spatial dynamics interact, our work provides a conceptual foundation of the factors likely also shaping more complex large scale models.

Declarations

Conflict of interest. The authors have no conflict of interest to declare.

Acknowledgements. We are grateful to Yuanxiao Gao for insightful discussions and helpful comments on the manuscript draft. We thank Shan Huang for helpful suggestions regarding figure 5. Both scientists were funded by the Swiss National Science Foundation (grant number: 211549).

References

Acevedo MA, Prosper O, Lopiano K, Ruktanonchai N, Caughlin TT, Martcheva M, et al. Spatial heterogeneity, host movement and mosquito-borne disease transmission. PloS one. 2015;10(6):e0127552.

Altizer S, Bartel R, Han BA. Animal migration and infectious disease risk. science. 2011;331(6015):296–302.

Anderson RM, May RM. Coevolution of hosts and parasites. Parasitology. 1982;85(2):411–426.

Antonis A, Kortekaas J, Kant J, Vloet R, Vogel-Brink A, Stockhofe N, et al. Vertical transmission of Rift Valley fever virus without detectable maternal viremia. Vector-borne and zoonotic diseases. 2013;13(8):601–606.

Antonovics J. Transmission dynamics: critical questions and challenges. Philosophical Transactions of the Royal Society B: Biological Sciences. 2017;372(1719):20160087.

Antonovics J, Wilson AJ, Forbes MR, Hauffe HC, Kallio ER, Leggett HC, et al. The evolution of transmission mode. Philosophical Transactions of the Royal Society B: Biological Sciences. 2017;372(1719):20160083.

Baudoin M. Host castration as a parasitic strategy. Evolution. 1975;p. 335–352.

Begon M, Bennett M, Bowers RG, French NP, Hazel S, Turner J. A clarification of transmission terms in host-microparasite models: numbers, densities and areas. Epidemiology & Infection. 2002;129(1):147–153.

Berngruber TW, Lion S, Gandon S. Spatial structure, transmission modes and the evolution of viral exploitation strategies. PLoS pathogens. 2015;11(4):e1004810.

Best A, Ashby B, White A, Bowers R, Buckling A, Koskella B, et al. Host–parasite fluctuating selection in the absence of specificity. Proceedings of the Royal Society B: Biological Sciences. 2017;284(1866).

Boulinier T, Kada S, Ponchon A, Dupraz M, Dietrich M, Gamble A, et al. Migration, prospecting, dispersal? What host movement matters for infectious agent circulation? Integrative and comparative biology. 2016;56(2):330–342.

Bradley CA, Altizer S. Parasites hinder monarch butterfly flight: implications for disease spread in migratory hosts. Ecology Letters. 2005;8(3):290–300.

Brenninger FA, Kovalov V, Kokko H. Sex-specific immunocompetence: resistance and tolerance can both be futile but not under the same circumstances. Evolution Letters. 2025;9(2):249–258.

Brophy T, Luong LT. The influence of infection status and parasitism risk on host dispersal and susceptibility to infection in Drosophila nigrospiracula. Parasitology. 2022;149(5):587–592.

Cattarino L, Rodriguez-Barraquer I, Imai N, Cummings DA, Ferguson NM. Mapping global variation in dengue transmission intensity. Science translational medicine. 2020;12(528):eaax4144.

Cottam EM, Wadsworth J, Shaw AE, Rowlands RJ, Goatley L, Maan S, et al. Transmission pathways of foot-and-mouth disease virus in the United Kingdom in 2007.

505 PLoS pathogens. 2008;4(4):e1000050.

506 Cressman R, Křivan V. Two-patch population models with adaptive dispersal: the
507 effects of varying dispersal speeds. Journal of mathematical biology. 2013;67(2):329–
508 358.

509 Da Ros CT, da Silva Schmitt C. Global epidemiology of sexually transmitted diseases.
510 Asian journal of andrology. 2008;10(1):110–114.

511 De Roode JC, Chi J, Rarick RM, Altizer S. Strength in numbers: high parasite bur-
512 dens increase transmission of a protozoan parasite of monarch butterflies (Danaus
513 plexippus). Oecologia. 2009;161:67–75.

514 Debeffe L, Morellet N, Verheyden-Tixier H, Hoste H, Gaillard JM, Cargnelutti B,
515 et al. Parasite abundance contributes to condition-dependent dispersal in a wild
516 population of large herbivore. Oikos. 2014;123(9):1121–1125.

517 van Dijk LJ, Ehrlén J, Tack AJ. The relationship between pathogen life-history traits
518 and metapopulation dynamics. New Phytologist. 2022;233(6):2585–2598.

519 Ebert D. The epidemiology and evolution of symbionts with mixed-mode transmission.
520 Annual Review of Ecology, Evolution, and Systematics. 2013;44(1):623–643.

521 Ewald PW. Host-parasite relations, vectors, and the evolution of disease severity.
522 Annual Review of Ecology and Systematics. 1983;14:465–485.

523 Ewald PW. Transmission modes and evolution of the parasitism-mutualism contin-
524 uum. Annals of the New York Academy of Sciences. 1987;503:295–306.

525 Fine PE. Vertical transmission of pathogens of invertebrates. In: Pathogens of Inver-
526 tebrates: Application in Biological Control and Transmission Mechanisms. Springer;
527 1984. p. 205–241.

528 Fulford GR, Roberts MG, Heesterbeek JA. The metapopulation dynamics of
529 an infectious disease: tuberculosis in possums. Theoretical population biology.

2002;61(1):15–29.

Gaff HD, Gross LJ. Modeling tick-borne disease: a metapopulation model. Bulletin of Mathematical Biology. 2007;69(1):265–288.

García-Ordóñez L, Pagán I. Vertical and horizontal transmission of plant viruses: two extremes of a continuum? npj Viruses. 2024;2(1):18.

Getahun M, Beyene B, Ademe A, Teshome B, Tefera M, Afework A, et al. Epidemiology of laboratory confirmed measles virus cases in the southern nations of Ethiopia, 2007–2014. BMC infectious diseases. 2017;17(1):87.

Grilli J, Barabás G, Allesina S. Metapopulation persistence in random fragmented landscapes. PLoS computational biology. 2015;11(5):e1004251.

Grumbach C, Reurik FN, Segura J, Franco D, Hilker FM. The effect of dispersal on asymptotic total population size in discrete-and continuous-time two-patch models. Journal of Mathematical Biology. 2023;87(4):60.

Guégan J, Morand S, Poulin R. Are there general laws in parasite community ecology? The emergence of spatial parasitology and epidemiology. Parasitism and ecosystems. 2005;p. 22–42.

Hagenaars T, Donnelly C, Ferguson N. Spatial heterogeneity and the persistence of infectious diseases. Journal of theoretical biology. 2004;229(3):349–359.

Hankins DG, Rosekrans JA. Overview, prevention, and treatment of rabies. In: Mayo Clinic Proceedings, vol. 79 Elsevier; 2004. p. 671–676.

Harbison CW, Bush SE, Malenke JR, Clayton DH. Comparative transmission dynamics of competing parasite species. Ecology. 2008;89(11):3186–3194.

Hickson RI, Mercer GN, Lokuge KM. A metapopulation model of tuberculosis transmission with a case study from high to low burden areas. PLoS One. 2012;7(4):e34411.

555 Hurst GD, Frost CL. Reproductive parasitism: maternally inherited symbionts in a
556 biparental world. Cold Spring Harbor perspectives in biology. 2015;7(5):a017699.

557 Jansen VA, Lloyd AL. Local stability analysis of spatially homogeneous solutions of
558 multi-patch systems. Journal of mathematical biology. 2000;41:232–252.

559 Jones EO, White A, Boots M. The evolution of host protection by vertically
560 transmitted parasites. Proceedings of the Royal Society B: Biological Sciences.
561 2011;278(1707):863–870.

562 Lafferty KD, Kuris AM. Parasitic castration: the evolution and ecology of body
563 snatchers. Trends in parasitology. 2009;25(12):564–572.

564 Laine AL, Hanski I. Large-scale spatial dynamics of a specialist plant pathogen in a
565 fragmented landscape. Journal of Ecology. 2006;94(1):217–226.

566 Lang JC, De Sterck H, Kaiser JL, Miller JC. Analytic models for SIR disease spread
567 on random spatial networks. Journal of Complex Networks. 2018;6(6):948–970.

568 Lipsitch M, Nowak MA, Ebert D, May RM. The population dynamics of vertically
569 and horizontally transmitted parasites. Proceedings of the Royal Society of London
570 Series B: Biological Sciences. 1995;260(1359):321–327.

571 Lipsitch M, Siller S, Nowak MA. The evolution of virulence in pathogens with vertical
572 and horizontal transmission. Evolution. 1996;50(5):1729–1741.

573 Lloyd AL, Jansen VA. Spatiotemporal dynamics of epidemics: synchrony in metapop-
574 ulation models. Mathematical biosciences. 2004;188(1-2):1–16.

575 Lloyd AL, Sattenspiel L. Spatiotemporal dynamics of measles: synchrony and persis-
576 tence in a disease metapopulation. In: Spatial ecology. Chapman and Hall/CRC;
577 2009. p. 277–298.

578 Massad E. Transmission rates and the evolution of pathogenicity. Evolution. 1987;p.
579 1127–1130.

McCallum H, Barlow N, Hone J. How should pathogen transmission be modelled? Trends in ecology & evolution. 2001;16(6):295–300.

Meibalan E, Marti M. Biology of malaria transmission. Cold Spring Harbor perspectives in medicine. 2017;7(3):a025452.

Messenger SL, Molineux IJ, Bull J. Virulence evolution in a virus obeys a trade off. Proceedings of the Royal Society of London Series B: Biological Sciences. 1999;266(1417):397–404.

Mo TA. Seasonal occurrence of Gyrodactylus derjavini (Monogenea) on brown trout, Salmo trutta, and Atlantic salmon, S. salar, in the Sandvikselva river, Norway. The Journal of parasitology. 1997;p. 1025–1029.

Pagán I, Montes N, Milgroom MG, García-Arenal F. Vertical transmission selects for reduced virulence in a plant virus and for increased resistance in the host. PLoS Pathogens. 2014;10(7):e1004293.

Pérez-Tris J, Bensch S. Dispersal increases local transmission of avian malarial parasites. Ecology Letters. 2005;8(8):838–845.

Post W, DeAngelis D, Travis C. Endemic disease in environments with spatially heterogeneous host populations. Mathematical Biosciences. 1983;63(2):289–302.

Riley S. Large-scale spatial-transmission models of infectious disease. Science. 2007;316(5829):1298–1301.

Roy B, Kirchner J. Evolutionary dynamics of pathogen resistance and tolerance. Evolution. 2000;54(1):51–63.

Ryder JJ, Miller MR, White A, Knell RJ, Boots M. Host-parasite population dynamics under combined frequency-and density-dependent transmission. Oikos. 2007;116(12):2017–2026.

Råberg L, Sim D, Read AF. Disentangling genetic variation for resistance and tolerance to infectious diseases in animals. Science. 2007;318(5851):812–814.

Shaw AK, Craft ME, Zuk M, Binning SA. Host migration strategy is shaped by forms of parasite transmission and infection cost. Journal of Animal Ecology. 2019;88(10):1601–1612.

Smith MJ, Telfer S, Kallio ER, Burthe S, Cook AR, Lambin X, et al. Host–pathogen time series data in wildlife support a transmission function between density and frequency dependence. Proceedings of the National Academy of Sciences. 2009;106(19):7905–7909.

Sutherland C, Elston D, Lambin X. A demographic, spatially explicit patch occupancy model of metapopulation dynamics and persistence. Ecology. 2014;95(11):3149–3160.

Szilágyi A, Meszéna G. Two-patch model of spatial niche segregation. Evolutionary Ecology. 2009;23(2):187–205.

Thrall PH, Antonovics J, Hall DW. Host and pathogen coexistence in sexually transmitted and vector-borne diseases characterized by frequency-dependent disease transmission. The American Naturalist. 1993;142(3):543–552.

Turner PE, Cooper VS, Lenski RE. Tradeoff between horizontal and vertical modes of transmission in bacterial plasmids. Evolution. 1998;52(2):315–329.

Xia Y, Bjørnstad ON, Grenfell BT. Measles metapopulation dynamics: a gravity model for epidemiological coupling and dynamics. The American Naturalist. 2004;164(2):267–281.

Zeng Q, Yu X, Ni H, Xiao L, Xu T, Wu H, et al. Dengue transmission dynamics prediction by combining metapopulation networks and Kalman filter algorithm. PLOS Neglected tropical diseases. 2023;17(6):e0011418.

629 Zilio G, Thiévent K, Koella JC. Host genotype and environment affect the trade-off
630 between horizontal and vertical transmission of the parasite Edhazardia aedis. BMC
631 evolutionary biology. 2018;18:1–9.

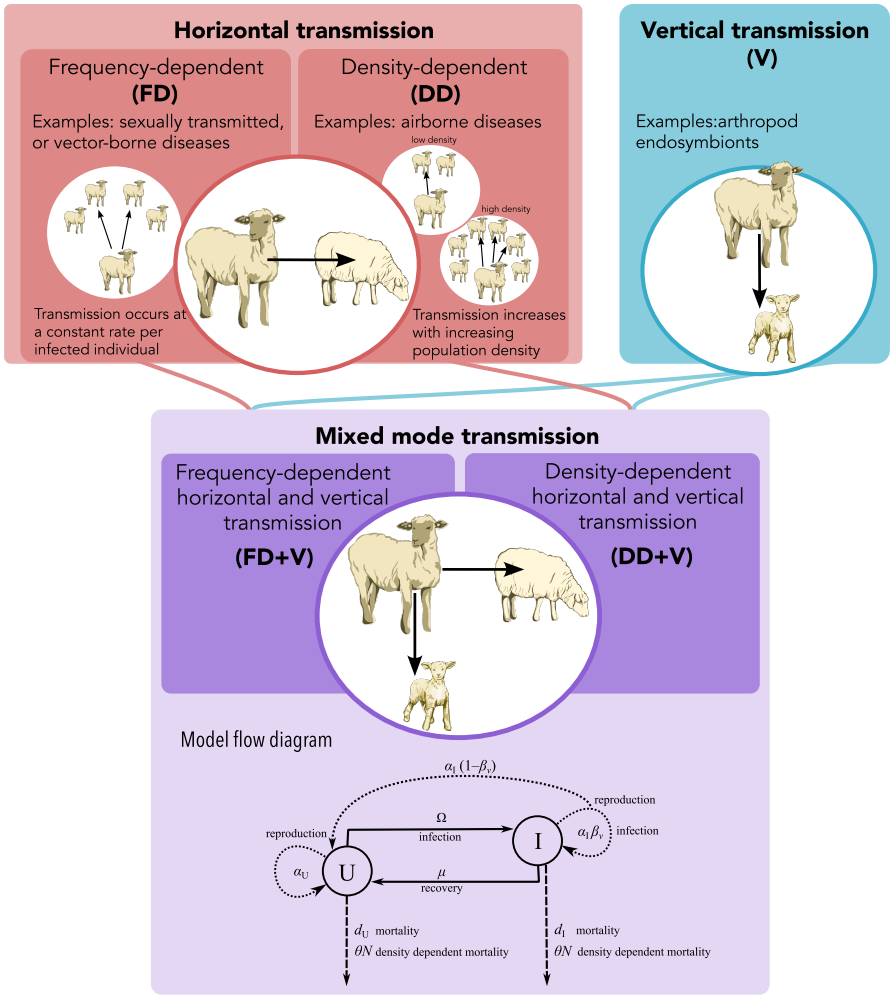

Fig. 1 Overview of the different transmission modes (and combinations thereof) considered. Transmission modes are broadly classified as horizontal (red box) or vertical (blue box). In the former, diseases transmit between two distinct individuals that are not necessarily related, while the later specifies that transmission occurs from parent to offspring. Some diseases use both modes to infect new hosts, which is usually referred to as mixed-mode transmission (purple box). The five distinct cases shown are: frequency-dependent horizontal transmission (FD), density-dependent horizontal transmission (DD), vertical transmission (V), mixed-mode transmission (FD+V), with frequency-dependent horizontal and vertical transmission and mixed-mode transmission (DD+V), with density-dependent horizontal and vertical transmission. At the bottom is a flow diagram corresponding to the presented model of mixed-mode transmission (equation 1). Meanings of the symbols are listed in Table 1. Solid lines correspond to infection gain or loss, while dashed lines mark mortality and dotted lines show processes corresponding to reproduction.

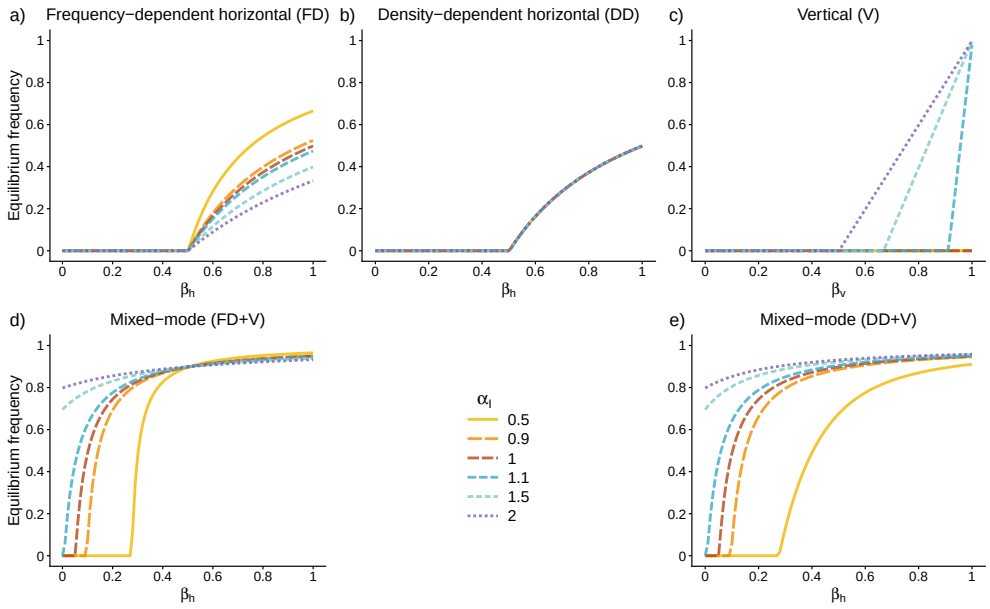

Fig. 2 Change in equilibrium frequency of infected individuals $\hat{I}$ with parasite transmission efficiency β_h, β_v and different per capita birth rate for infected individuals α_I for the different transmission mode scenarios: a) frequency-dependent horizontal transmission, b) density-dependent horizontal transmission, c) vertical transmission, d) mixed-mode transmission with frequency-dependent horizontal and vertical transmission and e) mixed-mode transmission with density-dependent horizontal and vertical transmission. Parameter values: $\alpha_U = 1$, $\mu = 0.002$, $d_U = 0.001$, $d_I = 0.002$, $\theta = 0.001$. The contact rate c was adjusted for the different cases of horizontal transmission. In a) and d) $c = 2$, while in b) and e) $c = 0.002$. In the mixed-mode transmission scenarios scenarios vertical transmission efficiency is set to $t_v = 0.9$. Population is initialized with $I = 1$ and $U = 199$ and run for $5 * 10^3$ time steps.

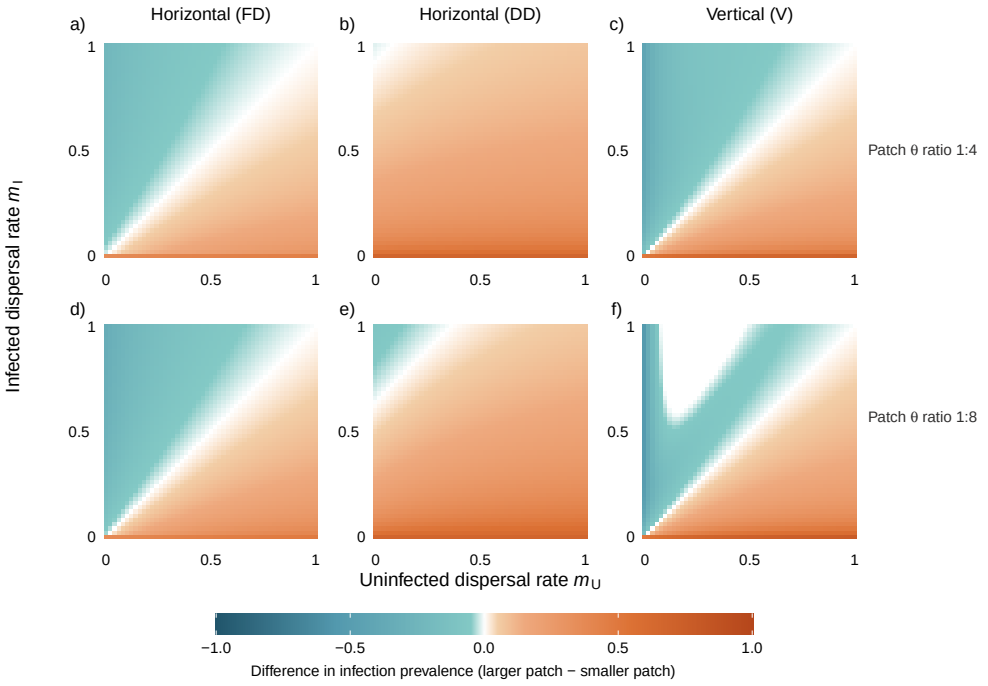

Fig. 3 Infection prevalence difference between two patches for varying dispersal rates, patch size ratios and transmission modes. Heatmap color shows the difference in infection prevalence between two patches (larger patch - smaller patch), where negative values indicate comparatively higher infection prevalence in the smaller patch, while positive values correspond to the larger patch containing higher infection prevalence. The parasite can transmit via frequency-dependent horizontal (a,d), density-dependent horizontal (b,e) or vertical transmission (c,f) modes. The difference in patch size is determined by θ, with ratio of 1:4 ($\theta_{large} = 0.001$, $\theta_{small} = 0.004$) in the top row (a-c) and 1:8 ($\theta_{large} = 0.001$, $\theta_{small} = 0.008$) in the bottom row (d-f). This θ difference results in the smaller patch containing $\sim$60% (a-c) and $\sim$45% (d-f) as many individuals as the larger patch, respectively. Small deviations from these percentages occur across transmission modes, reflecting the different infection dynamics arising in each case. Population is initialized with $I = 1$, $U = 199$ in the large patch and $I = 0$, $U = 200$ in the small patch and run for $2.5 * 10^3$ time steps. Other parameters used: $\alpha_U = 1.04$, $\alpha_I = 1.3$, $d_U = 0.001$, $d_I = 0.002$ $\beta_h = 0.9$, $\beta_v = 0.9$, $c_{FD} = 2$, $c_{DD} = 0.0035$ and $\mu = 0.002$.

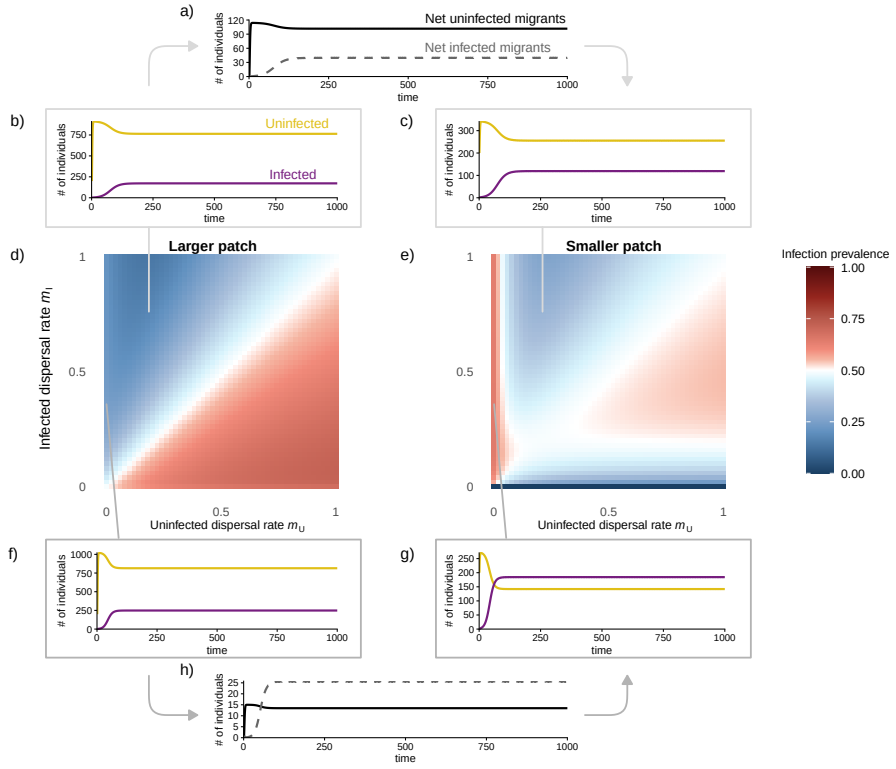

Fig. 4 Spread of a vertically transmitted parasite in two connected patches depending on dispersal rate of infected and uninfected individuals. Heatmap colors indicate infection prevalence in the larger $\theta_{large} = 0.001$ (d) and smaller patch $\theta_{small} = 0.004$ (e). The top gray boxes (a,c) exemplify the dynamics within each patch when uninfected and infected individuals disperse at rate $m_U = 0.2$ and $m_I = 0.75$, respectively. Due to the patch size difference, the smaller patch gains a net positive number of migrants (a), while the larger patch suffers the proportional net migration loss. Dispersal rates of $m_U = 0.02$ and $m_I = 0.4$ (bottom gray boxes; f,g), similarly produce a net positive migration from the larger to the smaller patch. Here, infected individuals disperse at a sufficiently high rate to outnumber the less dispersive uninfected migrants (h), resulting in a higher infection prevalence in the smaller compared to the larger patch (d,e,f,g). Population is initialized with $I = 1$, $U = 199$ (large patch), $I = 0$, $U = 200$ (small patch) and run for 10^3 time steps. Other parameters: $\alpha_U = 1.04$, $\alpha_I = 1.3$, $d_U = 0.001$, $d_I = 0.002$, $\beta_v = 0.9$ and $\mu = 0.002$.

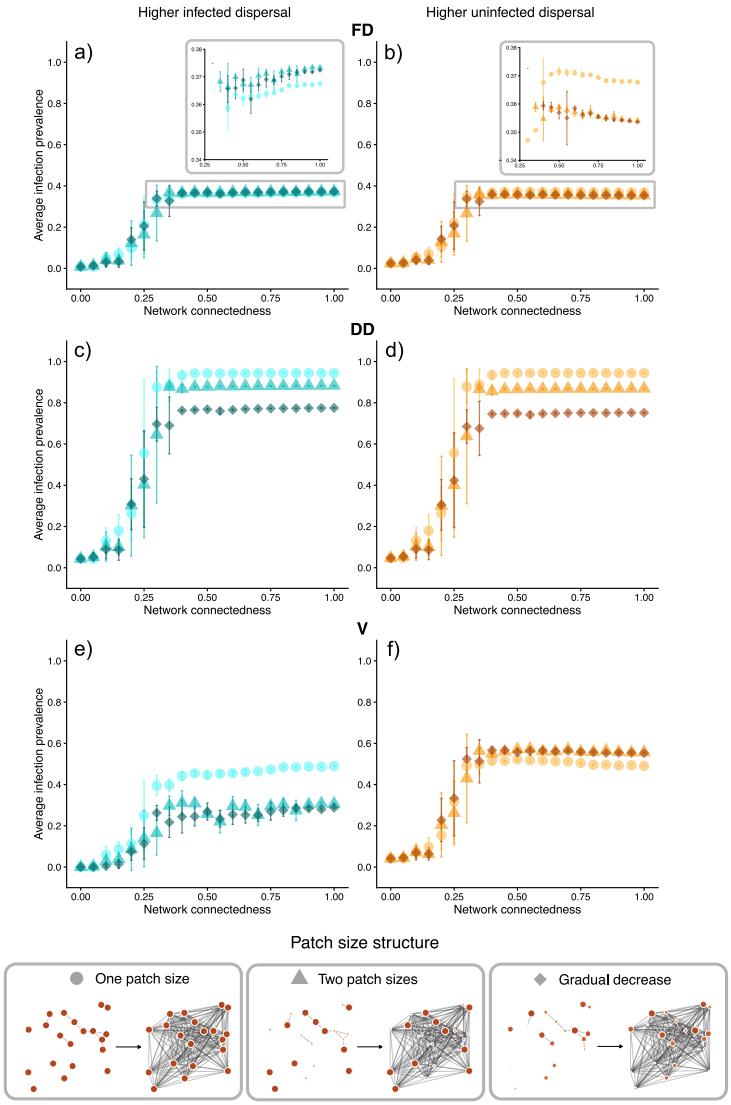

Fig. 5 Impact of network structure and dispersal on global infection prevalence for different transmission modes. We generate networks of 20 patches with distinct patch size configurations. Examples of such networks are shown (bottom gray boxes) for low levels of patch connectedness (left) to maximum connectedness $a = 1$ (right). The patch size ratios used to create the figures are 1:1 (where every patch in the network is the same size, $\theta = 0.001$) (dots), θ ratio 1:5 ($\theta_{larger} = 0.001$ and $\theta_{smaller} = 0.005$, where half of the patches contain ∼55% of the individuals in the larger patches) (triangles) or 1:10 (where patch sizes gradually decrease up to ∼40% the size of the largest patches, with two patches of each size, $\theta_n = 0.001n$ for $n = 1 : 10$) (diamond). Small deviations from these percentages occur across transmission modes, reflecting the different infection dynamics arising in each case. For each network, we track the global infection prevalence after 10^3 time steps for different parasite transmission modes, while also varying connectedness a of the patches. Calculations were repeated for five different randomly generated networks. We show the results for frequency-dependent horizontal (a,b), density-dependent horizontal (c,d) and vertical transmission (e,f) with dispersal propensities of $m_I = 0.75$ and $m_U = 0.25$ (a,c,e) and $m_I = 0.25$ and $m_U = 0.75$ (b,d,f). The gray boxes in a) and b) mark regions that are magnified in the insets to reveal patterns that are not visible at the scale of the full plots. Results for the other transmission modes are recorded in supplementary figure S10. The population is initialized with $I = 1$, $U = 199$, for one patch and $I = 0$, $U = 200$ in all other patches. Other parameters: $\alpha_U = 1.04$, $\alpha_I = 1.3$, $d_U = 0.001$, $d_I = 0.002$ $\beta_h = 0.9$, $\beta_v = 0.9$, $c_{FD} = 2$, $c_{DD} = 0.02$ and $\mu = 0.002$.

Supplementary Information

S1 Single patch dynamics

We first denote the UIU (uninfected-infected-uninfected) model for a well mixed population of asexually reproducing hosts. To compare infection dynamics resulting from five distinct transmission modes, we develop five separate models, each corresponding to a parasite using a different mode of transmission. We are not explicitly modeling parasite dynamics, but define a population of N host individuals, that can be infected I or uninfected U. Thus, $N = U + I$.

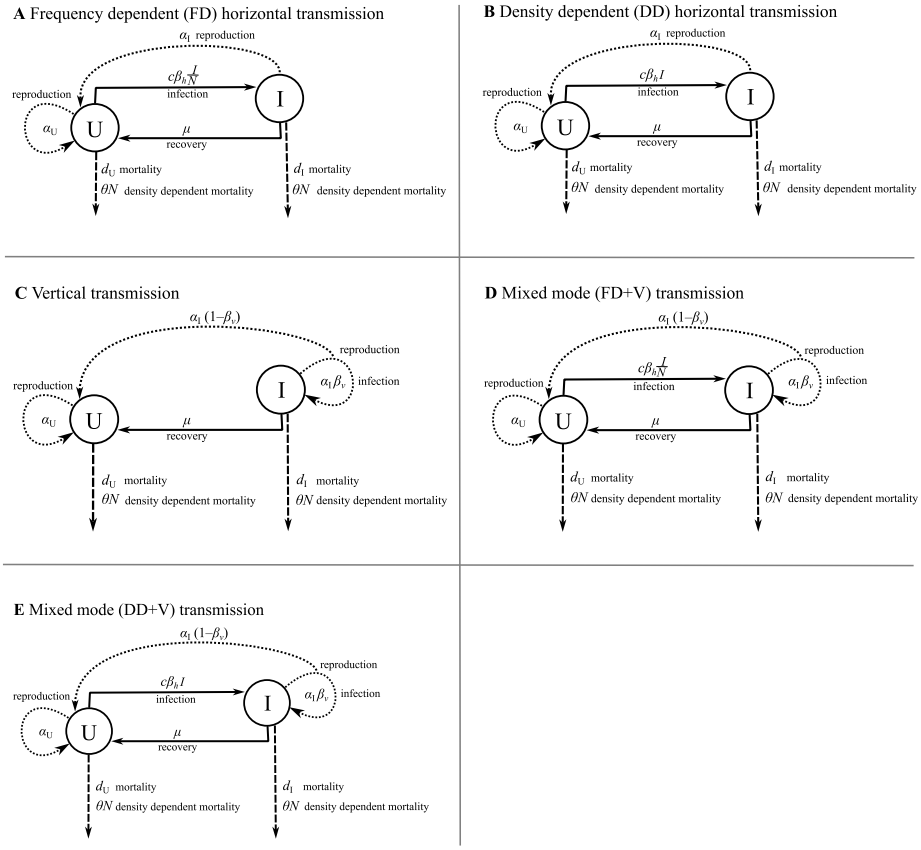

Fig. S1 Flow diagram corresponding to the UIU model for each considered transmission mode. Meaning of symbols are listed in Table 1. Solid lines correspond to parasite gain or loss, while dashed lines mark mortality and dotted lines show processes corresponding to reproduction.

S1.1 Horizontal transmission

S1.1.1 Frequency-dependent horizontal transmission

In sexually transmitted or vector borne diseases, horizontal transmission is commonly described as frequency-dependent (FD). The underlying assumption is that the parasite transmits at a constant rate per infected individual in the population, as is the case with sexual contacts or bites from a vector species that occur at a stable rate per infected individual. We denote the infection dynamics of a frequency-dependent horizontally transmitted parasite in a single well mixed host environment as

$$\begin{aligned} \frac{dU}{dt} &= \alpha_U U + \alpha_I I + \mu I - c\beta_h \frac{I}{N} U - d_U U - \theta N U, \\ \frac{dI}{dt} &= c\beta_h \frac{I}{N} U - \mu I - d_I I - \theta N I. \end{aligned} \tag{S1}$$

Here, α is the per capita growth rate and d the baseline mortality for uninfected and infected individuals, as indicated by the subscript $_U$ and $_I$, respectively. We assume that both fertility and mortality can differ with infection state, as infected individuals may experience higher mortality and reduced fertility compared to healthy con-specifics. The entire population is subject to the same density-dependent mortality, where increased crowding in the environment results in higher mortality. This effect is scaled by the parameter θ, modulating the strength of density-dependent mortality in a population. Individuals encounter one another at contact rate c, and the probability of coming into contact with an infected individual is given by the frequency of infected individuals in the population $\frac{I}{N}$. Upon contact with an infected individual, horizontal transmission of the parasite occurs with transmission efficiency β_h, resulting in infection of a previously uninfected individual. Infected individuals can recover and rejoin the uninfected state at recovery rate μ. See figure S1a for a flow diagram corresponding to equations S1, and Table 1 for a list of all symbols. Using equations S1, we can derive two different equilibrium states for the infection dynamics. In the first,

infection does not spread and the population consists of uninfected individuals:

$$\begin{aligned} \hat{U} &= \frac{\alpha_U - d_U}{\theta} \\ \hat{I} &= 0. \end{aligned} \tag{S2}$$

In the second, infected individuals spread in the population and reach a stable equilibrium with

$$\begin{aligned} \hat{U} &= -\frac{(\alpha_I-\mu)(-d_U^2-c\beta_h\alpha_I+d_I(c\beta_h-\alpha_U+\alpha_I-\mu)-\alpha_U\mu+\alpha_I\mu+d_U(d_I+\mu))}{(d_U-d_I+c\beta_h-\alpha_U+\alpha_I)^2\theta} \\ \hat{I} &= -\frac{(d_U-d_I+c\beta_h-\alpha_U-\mu)(-d_I^2-c\beta_h\alpha_I+d_I(c\beta_h-\alpha_U+\alpha_I-\mu)-\alpha_U\mu+\alpha_I\mu+d_U(d_I+\mu))}{(d_U-d_I+c\beta_h-\alpha_U+\alpha_I)^2\theta}. \end{aligned} \tag{S3}$$

Note how no trivial equilibrium exists, because when $I = 0$ and $U = 0$, it results that $N = U + I = 0$ and then $\frac{I}{N} = \frac{0}{0}$, which does not yield meaningful results. Thus, the system is not defined at point (0,0). For an example of the resulting dynamics of the system, see the corresponding phase portrait (figure S2).

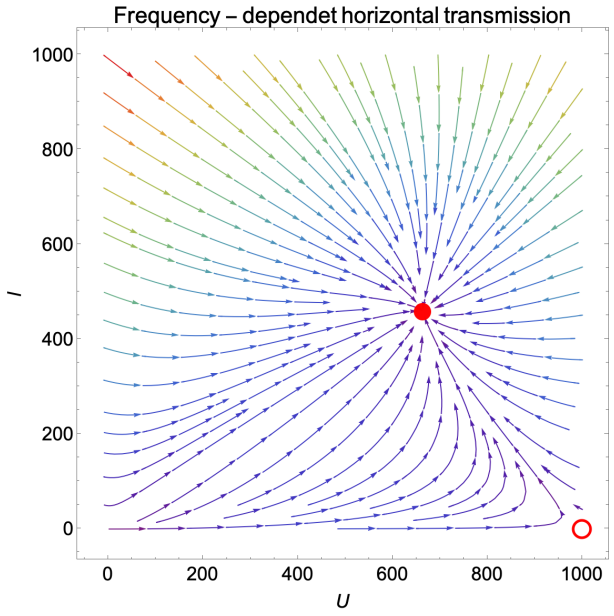

Fig. S2 Phase portrait with stability markers (red circles) for equilibria. The filled circle corresponds to the stable, the open circle to the unstable equilibrium calculated with parameters $\alpha_U = 1$, $\alpha_I = 1.3$, $d_U = 0.001$, $d_I = 0.002$, $\beta_h = 0.95$, $c = 2$, $\mu = 0.00003$ and $\theta = 0.001$.

S1.1.2 Density-dependent horizontal transmission

Compared to frequency-dependent transmission, density-dependent (DD) horizontal transmission captures the dynamics of parasites whose infectiousness increases with the density of individuals in an area. This is the case, for example, in diseases that are airborne or waterborne. We define the infection dynamics for such a case in a single patch as

$$\begin{aligned} \frac{dU}{dt} &= \alpha_U U + \alpha_I I + \mu I - c\beta_h IU - d_U U - \theta NU, \\ \frac{dI}{dt} &= c\beta_h IU - \mu I - d_I I - \theta NI. \end{aligned} \tag{S4}$$

Transmission of infection rises as population density increases (density-dependent or mass-action infection). Thus, the chance of a new infection is proportional to the number of infected and uninfected individuals in the population IU and scaled by the contact rate c and transmission efficiency of the parasite β_h. All other symbols and dynamics are identical to the frequency-dependent case. See the complementary flow diagram in figure S1b and Table 1 for a list of all symbols. For this system of equations, we can derive four different equilibrium states. In addition to the trivial equilibrium ($\hat{U} = 0$, $\hat{I} = 0$), there are three more equilibrium points:

$$\begin{aligned} \hat{U} &= \frac{\alpha_U - d_U}{\theta}, \\ \hat{I} &= 0, \end{aligned} \tag{S5}$$

$$\begin{aligned} \hat{U} &= \frac{1}{2c^2\beta_h^2}(\Big(- d_U + d_I + \alpha_U - \alpha_I)\theta + c\beta_h(d_I + \alpha_I + 2\mu\Big) - A, \\ \hat{I} &= \frac{1}{2c^2\beta_h^2\theta}\Big(c^2\beta_h^2(-d_I + \alpha_I) + (d_U - d_I - \alpha_U + \alpha_I)\theta^2 \\ &\quad - c\beta_h\theta(d_U - \alpha_U + 2(\alpha_I + \mu)) - c\beta_h A + \theta A\Big), \end{aligned} \tag{S6}$$

and

$$\begin{aligned} \hat{U} &= \frac{1}{2c^2\beta_h^2}\Big((-d_U + d_I + \alpha_U - \alpha_I)\theta + c\beta_h(d_I + \alpha_I + 2\mu\Big) + A, \\ \hat{I} &= \frac{1}{2c^2\beta_h^2\theta}\Big(c^2\beta_h^2(-d_I + \alpha_I) + (d_U - d_I - \alpha_U + \alpha_I)\theta^2 \\ &\quad - c\beta_h\theta(d_U - \alpha_U + 2(\alpha_I + \mu)) + c\beta_h A - \theta A\Big), \end{aligned} \tag{S7}$$

with $A = \sqrt{-4c^2\beta_h^2(d_I+\mu)(\alpha_I+\mu) + ((-d_U+d_I+\alpha_U-\alpha_I)\theta + c\beta_h(d_I+\alpha_I+2\mu))^2}$.
See figure S3 for a example of a corresponding phase portrait.

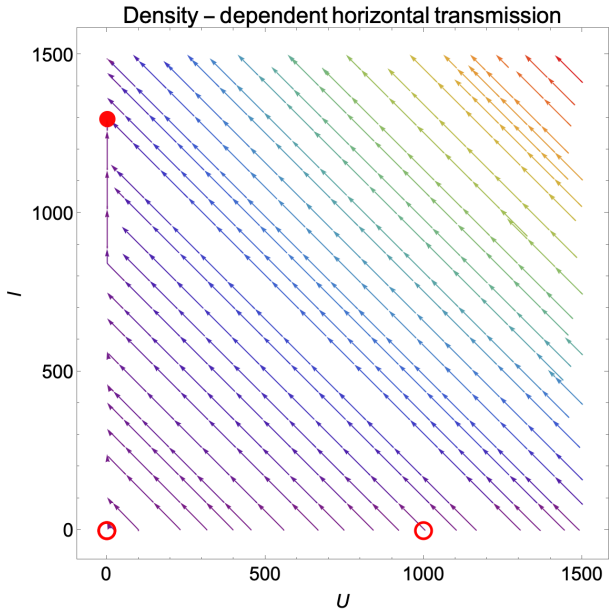

Fig. S3 Phase portrait with stability markers (red circles) for equilibria. The filled circle corresponds to the stable, the open circles to the unstable equilibrium calculated with parameters $\alpha_U = 1$, $\alpha_I = 1.3$, $d_U = 0.001$, $d_I = 0.002$, $\beta_h = 0.95$, $c = 2$, $\mu = 0.00003$ and $\theta = 0.001$. Note how the trivial equilibrium point is closely spaced with another equilibrium point, making the circles visually overlap and appear as a single circle.

S1.2 Vertical transmission

In this section, we consider the vertical transmission of a parasite in a host population. Examples of parasites that can transmit vertically include *Herpes simplex* virus and various endosymbionts inhabiting arthropods like *Wolbachia*. While the first example does not transmit only through the vertical mode, *Wolbachia* predominantly relies on vertical transmission. We define the infection dynamics with a parasite that exclusively

transmits vertically as

$$\begin{aligned}\frac{dU}{dt} &= \alpha_U U + \alpha_I(1-\beta_v)I + \mu I - d_U U - \theta N U,\\ \frac{dI}{dt} &= \alpha_I \beta_v I - \mu I - d_I I - \theta N I.\end{aligned} \tag{S8}$$

Because transmission of the parasite is exclusively vertical in this model, we assume that only infected individuals can birth infected individuals and thus, uninfected individuals cannot acquire the infection throughout their life. Vertical transmission efficiency is denoted by β_v, representing the proportion of offspring that inherit the parasite from an infected parent. The remaining proportion $1-\beta_v$ consists of offspring that did not inherit the parasite due to transmission failure and is instead added to the number of uninfected individuals in the population. Infected individuals can recover and lose the infection at rate μ, equivalent to the assumption in the previously described cases of horizontal transmission. All other dynamics are identical to the scenarios with horizontal transmission. See figure S1c for a flow diagram corresponding to equations S8 and Table 1 for a list of all symbols. Equations S8 yield three equilibrium states. In addition to the a trivial equilibrium point, we can determine two more equilibria of the population:

$$\begin{aligned}\hat{U} &= \frac{\alpha_U - d_U}{\theta},\\ \hat{I} &= 0\end{aligned} \tag{S9}$$

and

$$\begin{aligned}\hat{U} &= \frac{((-1+\beta_v)\alpha_I - \mu)(d_I - \beta_v\alpha_I + \mu)}{(d_U - d_I - \alpha_U + \alpha_I)\theta},\\ \hat{I} &= -\frac{(d_U - d_I - \alpha_U + \beta_v\alpha_I - \mu)(d_I - \beta_v\alpha_I + \mu)}{(d_U - d_I - \alpha_U + \alpha_I)\theta}.\end{aligned} \tag{S10}$$

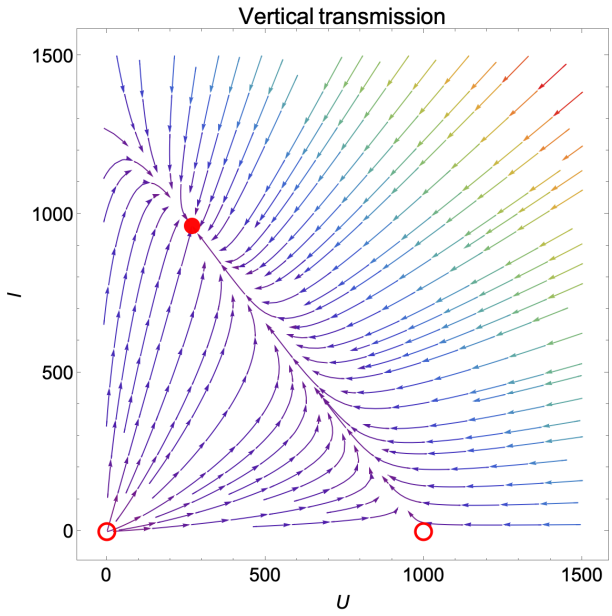

Fig. S4 Phase portrait with stability markers (red circles) for equilibria. The filled circle corresponds to the stable, the open circles to the unstable equilibrium calculated with parameters $\alpha_U = 1$, $\alpha_I = 1.3$, $d_U = 0.001$, $d_I = 0.002$, $\beta_v = 0.95$, $\mu = 0.00003$ and $\theta = 0.001$.

S1.3 Mixed-mode transmission (horizontal and vertical)

S1.3.1 frequency-dependent horizontal and vertical transmission (FD+V)

Some parasites are able to transmit via multiple modes, usually referred to as mixed-mode transmission. We consider parasites with mixed-mode transmission that utilize both a horizontal and a vertical pathway. We first denote the infection dynamics for a parasite that combines frequency-dependent horizontal and vertical transmission as

$$\begin{aligned} \frac{dU}{dt} &= \alpha_U U + \alpha_I(1-\beta_v)I + \mu I - d_U U - \theta N U - c\beta_h \frac{I}{N} U, \\ \frac{dI}{dt} &= \alpha_I \beta_v I + c\beta_h \frac{I}{N} U - \mu I - d_I I - \theta N I. \end{aligned} \tag{S11}$$

Here, parasites can transmit both horizontally and vertically, though transmission efficiency may vary by mode. It is possible that horizontal and vertical transmission are

equally efficient ($\beta_h = \beta_v$), or that transmission efficiency is higher via one mode compared to the other $\beta_h < \beta_v$ or $\beta_h > \beta_v$. Individuals can inherit the parasite (vertical) or get infected during their life (horizontal). All other dynamics mirror the previous equations considering parasites with a single transmission mode. See figure S1d for a flow diagram corresponding to equations S11, Table 1 for a list of all symbols. Similar to the scenario with only frequency-dependent horizontal transmission, in this mixed-mode transmission case, there is no trivial equilibrium, because the system cannot be defined when $\frac{I}{N} = \frac{0}{0}$. The equilibrium points of the system are

$$\begin{aligned} \hat{U} &= \frac{\alpha_U - d_U}{\theta}, \\ \hat{I} &= 0 \end{aligned} \tag{S12}$$

and

$$\begin{aligned} \hat{U} &= \frac{1}{(d_U - d_I + c\beta_h - \alpha_U + \alpha_I)^2\theta} \left(((\beta_v - 1)\alpha_I - \mu)C\right), \\ \hat{I} &= -\frac{1}{(d_U - d_I + c\beta_h - \alpha_U + \alpha_I)^2\theta} \left(d_U - d_I + c\beta_h - \alpha_U + \beta_v\alpha_I - \mu\right) C \end{aligned} \tag{S13}$$

with $C = (-d_I^2 - \alpha_I(c\beta_h - \beta_v\alpha_U + \beta_v\alpha_I) + d_I(c\beta_h - \alpha_U + \alpha_I + \beta_v\alpha_I - \mu) + (\alpha_I - \alpha_U)\mu + d_U(d_I - \beta_v\alpha_I + \mu))$.

See figure S5 for a corresponding phase portrait.

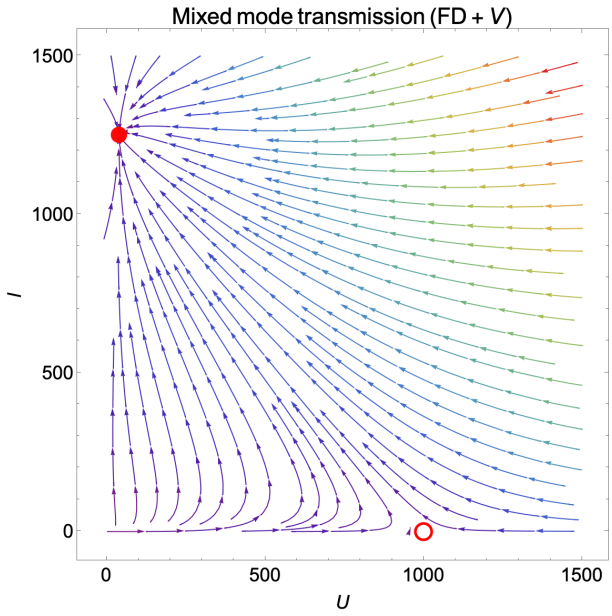

Fig. S5 Phase portrait with stability markers (red circles) for equilibria. The filled circle corresponds to the stable, the open circles to the unstable equilibrium calculated with parameters $\alpha_U = 1$, $\alpha_I = 1.3$, $d_U = 0.001$, $d_I = 0.002$, $\beta_h = 0.95$,$\beta_v = 0.95$, $c = 2$, $\mu = 0.00003$ and $\theta = 0.001$.

S1.3.2 Density-dependent horizontal and vertical transmission (DD+V)

Next, we define the infection dynamics for a parasite that uses a combination of density-dependent horizontal and vertical transmission as

$$\begin{aligned} \frac{dU}{dt} &= \alpha_U U + \alpha_I(1-\beta_v)I + \mu I - d_U U - \theta N U - c\beta_h I U, \\ \frac{dI}{dt} &= \alpha_I \beta_v I + c\beta_h I U - \mu I - d_I I - \theta N I. \end{aligned} \tag{S14}$$

All symbols (Table 1) and assumptions follow the previous cases. See figure S1e for a flow diagram corresponding to equations S14. We derive four equilibrium points (figure S6) for this system of equations. One is trivial, the others are:

$$\begin{aligned} \hat{U} &= \frac{\alpha_U - d_U}{\theta}, \\ \hat{I} &= 0, \end{aligned} \tag{S15}$$

$$\hat{U} = \frac{1}{2c^2\beta_h^2}\Big(cd_I\beta_h + c\beta_h\alpha_I - 2c\beta_h\beta_v\alpha_I - d_U\theta + d_I\theta + \alpha_U\theta - \alpha_I\theta + 2c\beta_h\mu - B\Big),$$
$$\hat{I} = \frac{1}{2c^2\beta_h^2\theta}\Big(- c^2d_I\beta_h^2 + c^2\beta_h^2\alpha_I - cd_U\beta_h\theta + c\beta_h\alpha_U\theta - 2c\beta_h\alpha_I\theta + 2c\beta_h\beta_v\alpha_I\theta$$
$$+ d_U\theta^2 - d_I\theta^2 - \alpha_U\theta^2 + \alpha_I\theta^2 - 2c\beta_h\theta\mu - c\beta_hB + \theta B\Big). \tag{S16}$$

and

$$\hat{U} = \frac{1}{2c^2\beta_h^2}\Big(cd_I\beta_h + c\beta_h\alpha_I - 2c\beta_h\beta_v\alpha_I - d_U\theta + d_I\theta + \alpha_U\theta - \alpha_I\theta + 2c\beta_h\mu + B\Big),$$
$$\hat{I} = \frac{1}{2c^2\beta_h^2\theta}\Big(- c^2d_I\beta_h^2 + c^2\beta_h^2\alpha_I - cd_U\beta_h\theta + c\beta_h\alpha_U\theta - 2c\beta_h\alpha_I\theta + 2c\beta_h\beta_v\alpha_I\theta$$
$$+ d_U\theta^2 - d_I\theta^2 - \alpha_U\theta^2 + \alpha_I\theta^2 - 2c\beta_h\theta\mu + c\beta_hB - \theta B\Big) \tag{S17}$$

with $B = \sqrt{4c^2\beta_h^2((-1+\beta_v)\alpha_I - \mu)(d_I - \beta_v\alpha_I + \mu) + ((-d_U + d_I + \alpha_U - \alpha_I)\theta + c\beta_h(d_I + \alpha_I - 2\beta_v\alpha_I + 2\mu))^2}$.

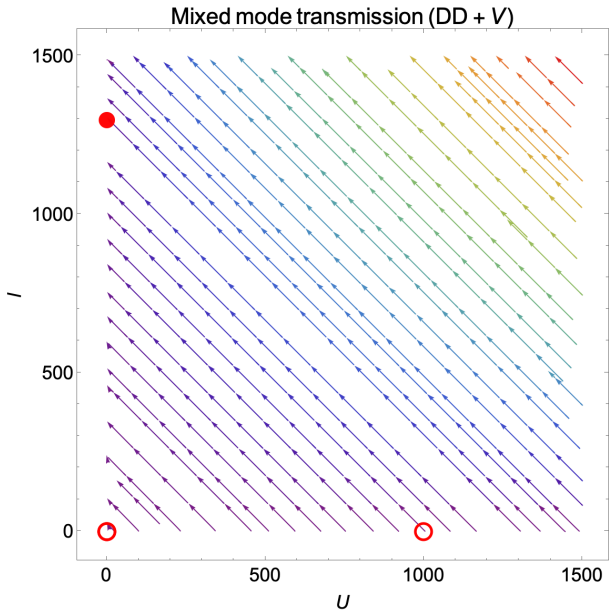

Fig. S6 Phase portrait with stability markers (red circles) for equilibria. The filled circle corresponds to the stable, the open circles to the unstable equilibrium calculated with parameters $\alpha_U = 1$, $\alpha_I = 1.3$, $d_U = 0.001$, $d_I = 0.002$, $\beta_h = 0.95$, $\beta_v = 0.95$, $c = 2$, $\mu = 0.00003$ and $\theta = 0.001$. Note how the trivial equilibrium point is closely spaced with another equilibrium point, making the circles visually overlap and appear as a single circle.

S2 Mainland-island models

As an example, consider 2 patches i and j, where dispersal from i to j is just as likely as dispersal from j to i, meaning that the habitats are equally well connected. This symmetrical connectedness is captured by the connection matrix $\mathbf{S}$ below.

$$\mathbf{S} = \begin{bmatrix} -1 & 1 \\ 1 & -1 \end{bmatrix} \tag{S18}$$

The elements of the matrix, s_{ij}, describes the proportion of dispersers from patch i that relocate to patch j. For the connection matrix above (equation S18) $s_{1,2} = s_{2,1} = 1$, meaning that all dispersing individuals of patch 1 move to patch 2 and vice versa. The diagonal elements in matrix $\mathbf{S}$ captures the corresponding emigration of dispersers from each patch with $s_{ii} = -1$, $i = 1, 2$, indicating that all

dispersers from i successfully leave patch i.

In our model we consider that infection state can influence dispersal propensity. Infected individuals, for example, may become more or less likely to move to a new patch compared to uninfected con-specifics (Bradley and Altizer 2005; Debeffe et al. 2014; Brophy and Luong 2022). To account for this, we define two different dispersal propensities m_U and m_I, referring to uninfected and infected individuals, respectively. Matrix $\mathbf{M}$ tracks the dispersal probability of different types of individuals:

$$\mathbf{M} = \begin{bmatrix} m_U & 0 \\ 0 & m_I \end{bmatrix} \tag{S19}$$

Here, $m_{1,2} = 0$ and $m_{2,1} = 0$ (equation S19) further implies that individuals cannot get infected or recover during dispersal, which corresponds to our model assumption that infection status can only change within the dynamics of a patch.

To evaluate the possibility that two habitats are of different sizes, we assign patch specific density-dependent mortality θ_i, θ_j. A larger density-dependent mortality θ, corresponds to a smaller habitat, where individual mortality increases at comparatively lower levels of crowding. Note that this form of population size regulation does not impose a strict carrying capacity. Instead, the penalty for crowding increases with larger population size θN. Here we explicitly note down the equations for the two-patch dynamics between patch i and j.

In the following, we denote the equations for each transmission mode (equations S1, S4, S8, S11 and S14) and expand them to a two-patch system, where two habitats are connected by dispersing individuals (as described above).

S2.1 Frequency-dependent horizontal transmission and in a two-patch system

In the FD horizontal transmission scenario, in a world with two equally well connected patches j and i equation 1 boils down to:

$$\begin{aligned}
\frac{dU_j}{dt} &= \alpha_U U_j + \alpha_I I_j + \mu I_j - \theta_j N_j U_j - c\beta_h \frac{I_j}{N_j} U_j - d_U U_j + m_U(U_i - U_j),\\
\frac{dI_j}{dt} &= c\beta_h \frac{I_j}{N_j} U_j - \theta_j N_j I_j - \mu I_j - d_I I_j + m_I(I_i - I_j),\\
\frac{dU_i}{dt} &= \alpha_U U_i + \alpha_I I_i + \mu I_i - \theta_i N_i U_i - c\beta_h \frac{I_i}{N_i} U_i - d_U U_i + m_U(U_j - U_i),\\
\frac{dI_i}{dt} &= c\beta_h \frac{I_i}{N_i} U_i - \theta_i N_i I_i - \mu I_i - d_I I_i + m_I(I_j - I_i).
\end{aligned} \tag{S20}$$

S2.2 Density-dependent horizontal transmission and in a two-patch system

Now we repeat these considerations for density-dependent horizontal transmission. However, we now note down the dynamics for only one patch in the two-patch system, as the equations are equivalent for the second patch, except for swapped indices i for j:

$$\begin{aligned}
\frac{dU_j}{dt} &= \alpha_U U_j + \alpha_I I_j + \mu I_j - \theta_j N_j U_j - c\beta_h I_j U_j - d_U U_j + m_U(U_i - U_j),\\
\frac{dI_j}{dt} &= c\beta_h I_j S_j - \theta_j N_j I_j - \mu I_j - d_I I_j + m_I(I_i - I_j).
\end{aligned} \tag{S21}$$

This describes the change in frequency of infected and susceptible individuals in patches i and j.

S2.3 Vertical transmission and in a two-patch system

We can derive the dynamics when the parasite is transmitted exclusively vertically (written down as an example in just one patch, dynamics in the second patch are

equivalent but with swapped i and j):

$$\begin{aligned}\frac{dU_j}{dt} &= \alpha_U U_j + \alpha_I(1-\beta_v)I_j + \mu I_j - \theta_j N_j U_j - d_U U_j + m_U(U_i - U_j),\\ \frac{dI_j}{dt} &= \alpha_I \beta_v I_j - \theta_j N_j I_j - \mu I_j - d_I I_j + m_I(I_i - I_j),\end{aligned} \tag{S22}$$

S2.4 Mixed-mode transmission (FD+V) and in a two-patch system

For mixed-mode (FD+V) transmission of the parasite, the equations to describe the dynamics in the different patches are:

$$\begin{aligned}\frac{dU_j}{dt} &= \alpha_U U_j + \alpha_I(1-\beta_v)I_j + \mu I_j - \theta_j N_j U_j - c\beta_h \frac{I_j}{N_j} U_j - d_U U_j + m_U(U_i - U_j),\\ \frac{dI_j}{dt} &= \alpha_I \beta_v I_j + c\beta_h \frac{I_j}{N_j} U_j - \theta_j N_j I_j - \mu I_j - d_I I_j + m_I(I_i - I_j).\end{aligned} \tag{S23}$$

The dynamics in the second patch are equivalent but with swapped i and j.

S2.5 Mixed-mode transmission and in a two-patch system

Lastly, in the case of mixed-mode transmission with density-dependent horizontal and vertical transmission the two patch dynamics can be denoted as:

$$\begin{aligned}\frac{dU_j}{dt} &= \alpha_U U_j + \alpha_I(1-\beta_v)I_j + \mu I_j - \theta_j N_j U_j - c\beta_h I_j U_j - d_U U_j + m_U(U_i - U_j),\\ \frac{dI_j}{dt} &= \alpha_I \beta_v I_j + c\beta_h I_j U_j - \theta_j N_j I_j - \mu I_j - d_I I_j + m_I(I_i - I_j).\end{aligned} \tag{S24}$$

Again, the dynamics in the second patch are equivalent but with swapped i and j.

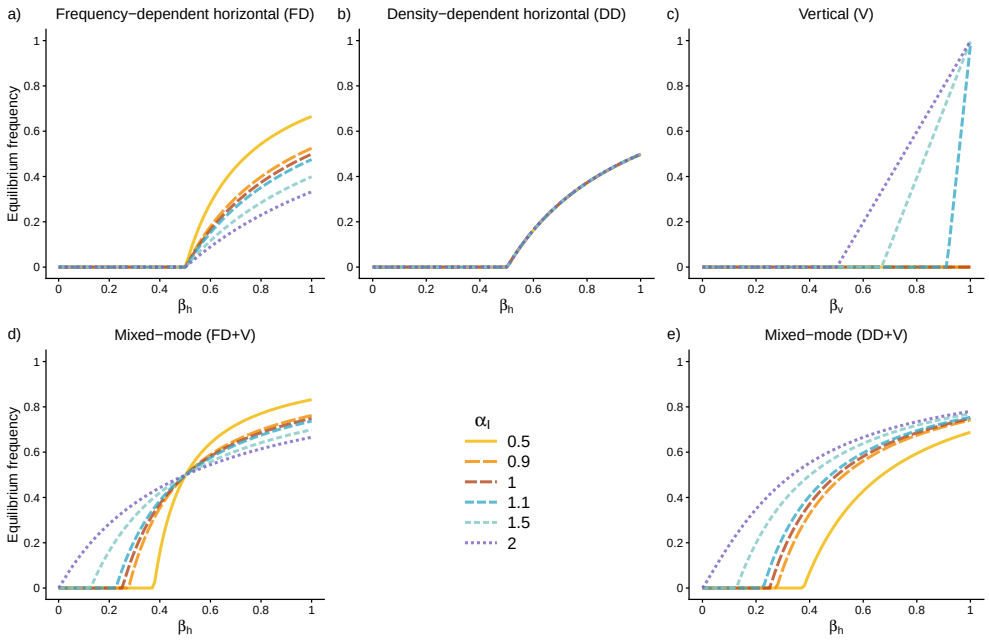

Fig. S7 Change in equilibrium frequency of infected individuals $\hat{I}$ with parasite transmission efficiency β and different per capita birth rate for infected individuals α_I for the different transmission mode scenarios: a) frequency-dependent horizontal transmission, b) density-dependent horizontal transmission, c) vertical transmission, d) mixed-mode transmission with frequency-dependent horizontal and vertical transmission and e) mixed-mode transmission with density-dependent horizontal and vertical transmission. Parameter values: $\alpha_U = 1$, $\mu = 0.002$, $d_U = 0.001$, $d_I = 0.002$, $\theta = 0.001$. The contact rate c was adjusted for the different cases of horizontal transmission. In a) and d) $c = 2$, while in b) and e) $c = 0.002$. In the mixed-mode transmission scenarios scenarios vertical transmission efficiency is set to $t_v = 0.5$. Population is initialized with $I = 1$ and $U = 199$.

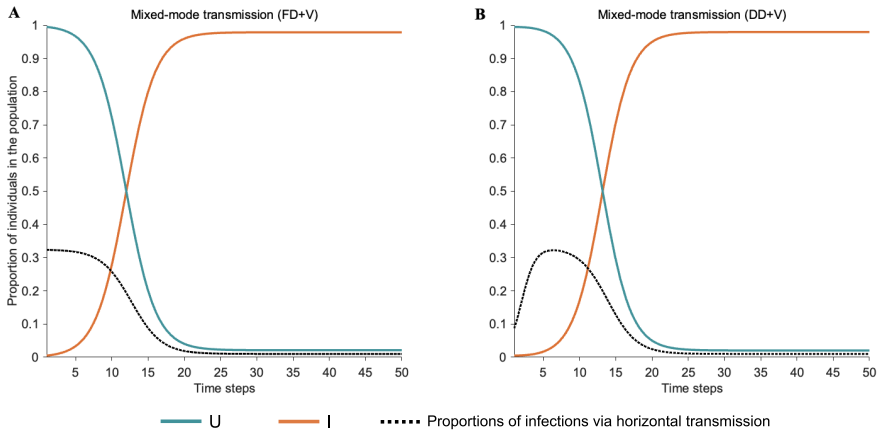

Fig. S8 Proportion of infections facilitated by horizontal transmission (dashed line) in the two mixed-mode scenarios compared to the change the proportion of uninfected (blue line) and infected (orange line) individuals in the population over time. Population is initialized with $I = 1$ and $U = 199$ and run for 50 time steps. Parameter values: $\alpha_U = 1.04$, $\alpha_I = 1.04$, $\mu = 0.0001$, $d_U = 0.001$, $d_I = 0.002$, $\beta_h = 0.99$, $\beta_v = 0.99$ and $\theta = 0.001$, in A) $c = 0.5$ and in B) $c = 0.0005$.

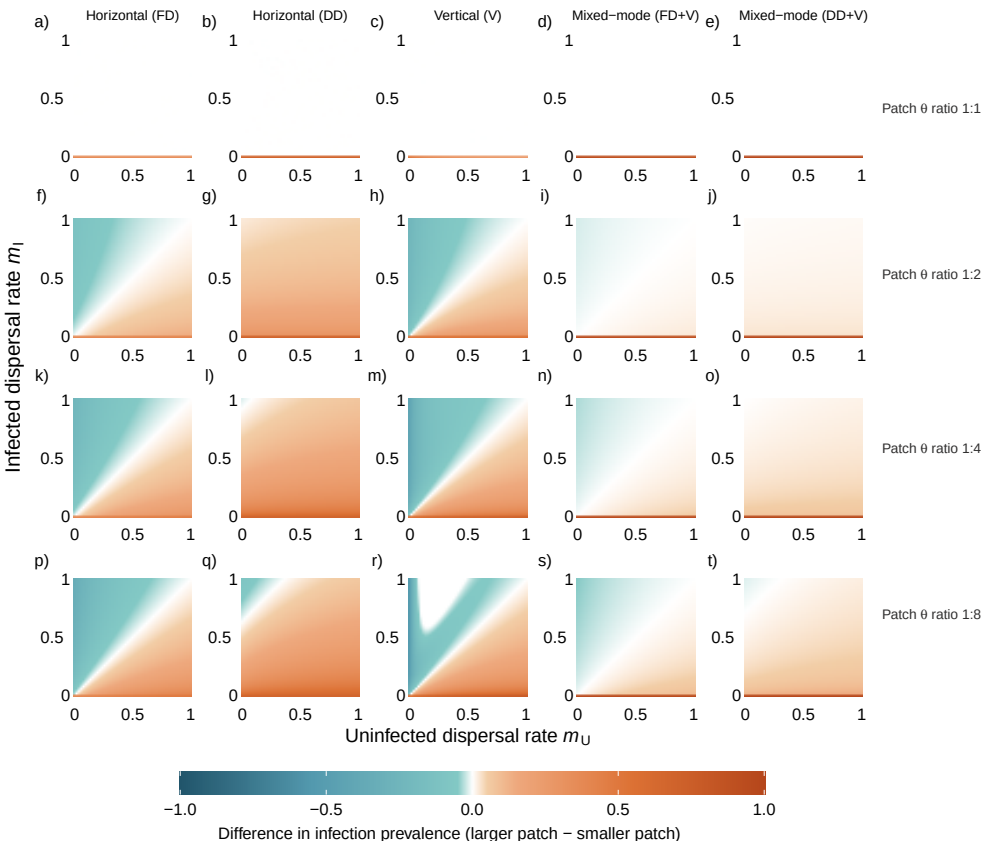

Fig. S9 Infection prevalence difference between two patches for varying dispersal rates, patch size ratios and transmission modes. Heatmap color shows the difference in infection prevalence between two patches (larger patch - smaller patch), where negative values indicate comparatively higher infection prevalence in the smaller patch, while positive values correspond to the larger patch containing higher infection prevalence. The parasite can transmit via frequency-dependent horizontal (a,f,k,p), density-dependent horizontal (b,g,l,q), vertical transmission (c,h,m,r), mixed-mode transmission including frequency-dependent horizontal and vertical transmission (d,i,n,s) or mixed-mode transmission including density-dependent horizontal and vertical transmission (e,j,o,t). In the top row (a-e) patches are the same size, resulting in no difference in infection prevalence, except in the cases, where infected individuals do not disperse $m_I = 0$ and the infection only spreads inside one patch. The difference in size increases with each descending row, with patch θ ratio 1:2 ($\theta_{large} = 0.001$, $\theta_{small} = 0.002$), 1:4 ($\theta_{large} = 0.001$, $\theta_{small} = 0.004$) and 1:8 ($\theta_{large} = 0.001$, $\theta_{small} = 0.008$). This difference in θ results in the smaller patch containing 75%, 60% and 45% as many individuals as the larger patch, respectively. Small deviations from these percentages occur across transmission modes, reflecting the different infection dynamics arising in each case, as, for example, a larger number of infected individuals will lead to higher mortality in a patch. Population is initialized with $I = 1$ and $U = 199$ in the large patch and $I = 0$, $U = 200$ in the small patch. Dynamics are run for $2.5 * 10^3$ time steps. Other parameters used: $\alpha_U = 1.04$, $\alpha_I = 1.3$, $d_U = 0.001$, $d_I = 0.002$ $\beta_h = 0.9$, $\beta_v = 0.9$, $c_{FD} = 2$, $c_{DD} = 0.0035$ and $\mu = 0.002$.

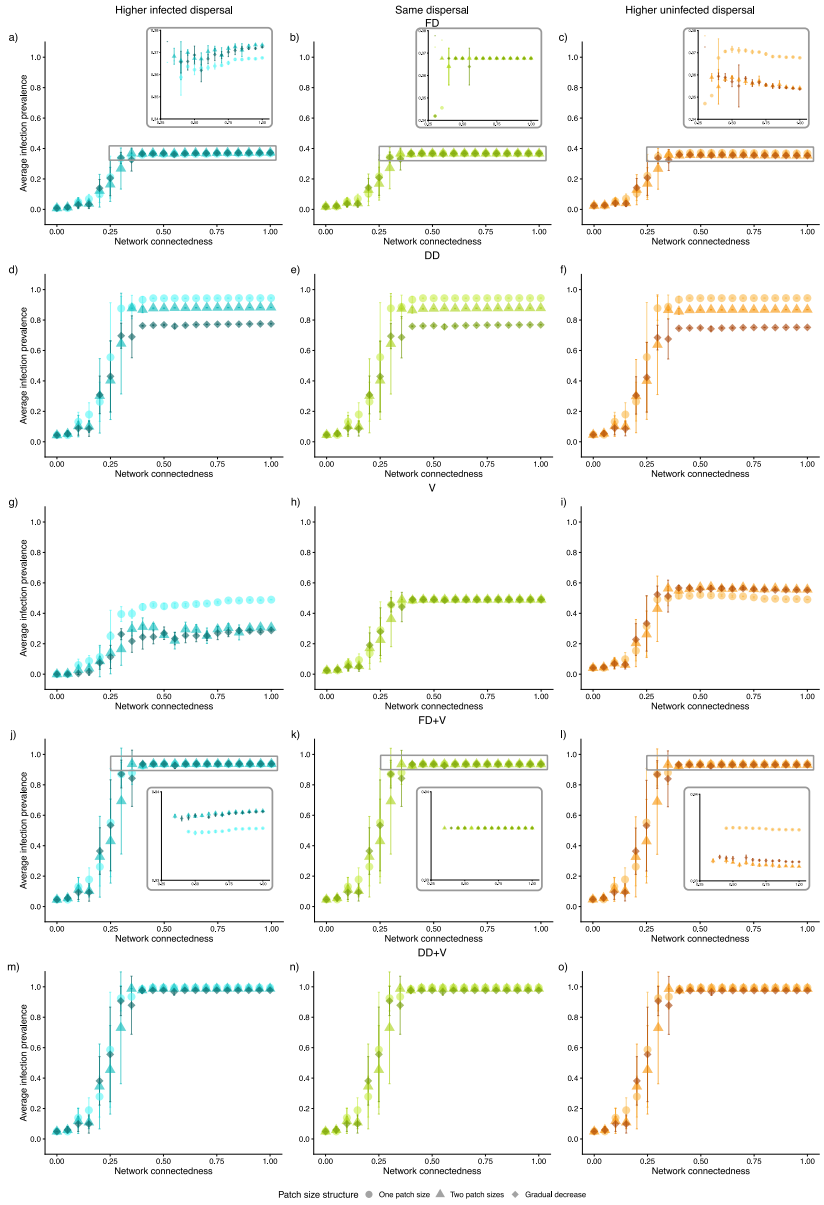

Fig. S10 Impact of network structure and dispersal propensity on global infection prevalence in randomly generated networks. We generate networks of 20 patches, where patch size ratios were either all the same 1:1 with $\theta = 0.001$ (circles), θ ratio 1:5 ($\theta_{larger} = 0.001$ and $\theta_{smaller} = 0.005$, where half of the patches contain ∼55% of the individuals in the larger patches) (triangles) or 1:10 (where patch sizes gradually decrease up to ∼40% the size of the largest patches, with two patches of each size, $\theta_n = 0.001n$ for $n = 1 : 10$) (diamond). Small deviations from these percentages occur across transmission modes, reflecting the different infection dynamics arising in each case. For each network, we track the global infection prevalence after 10^3 time steps for all parasite transmission modes, while varying connectedness a of the patches: FD (a-c), DD (d-f), V (g-i), FD+V (j-l), DD+V (m-o). Calculations were repeated for five different randomly generated networks and for three different combinations of dispersal propensities: (left column) $m_U = 0.25$ and $m_I = 75$; (middle column) $m_U = 0.5$ and $m_I = 0.5$; (right column) $m_U = 0.75$ and $m_I = 25$. Each gray box shows a magnified view of the regions indicated by the corresponding smaller gray box. All transmission modes are applied to each network. Population is initialized with $I_1 = 1$, $U_1 = 199$, for one patch and $I_n = 0$, $U_n = 200$ in all other patches. Other parameters: $\alpha_U = 1.04$, $\alpha_I = 1.3$, $d_U = 0.001$, $d_I = 0.002$, $\beta_h = 0.9$, $\beta_v = 0.9$, $c_{FD} = 2$, $c_{DD} = 0.02$, $\mu = 0.002$.

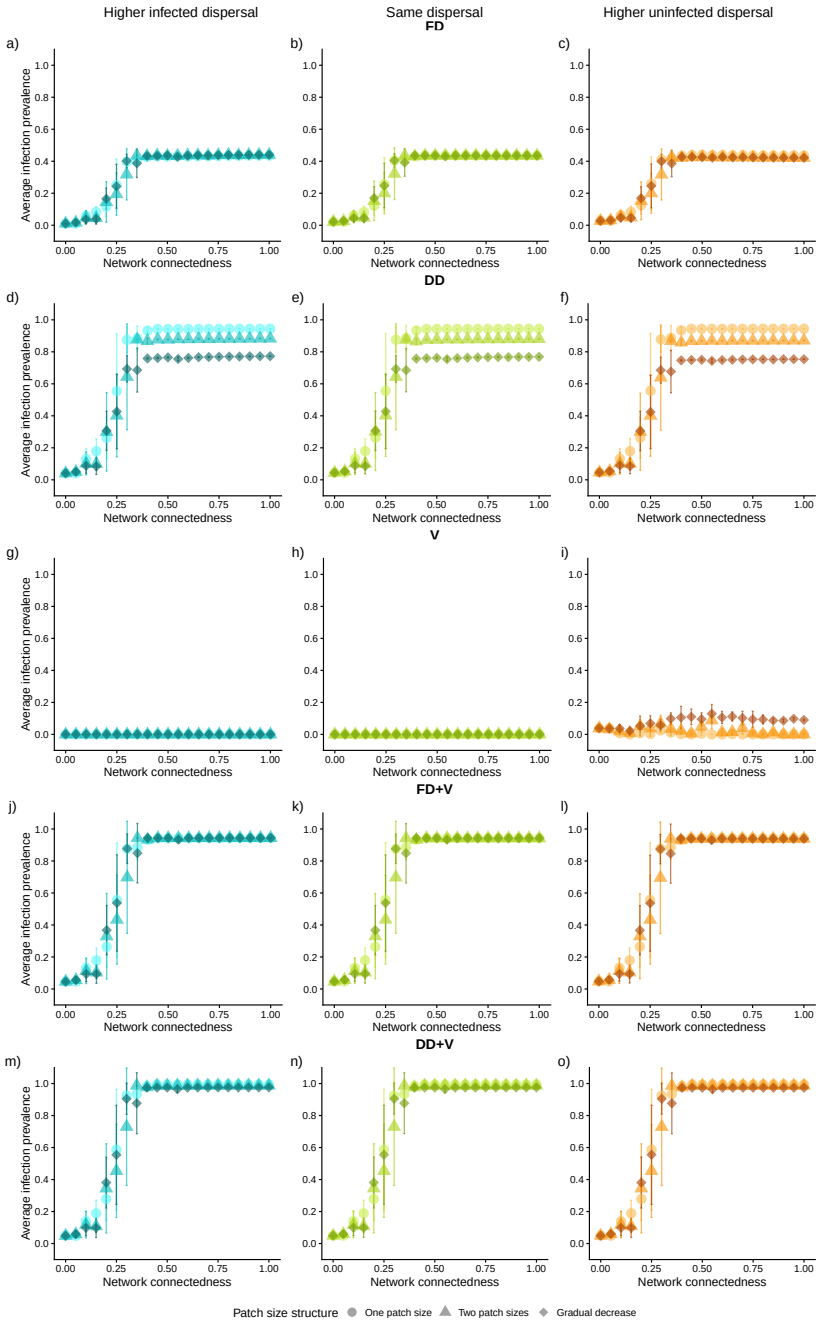

Fig. S11 Impact of network structure and dispersal propensity on global infection prevalence in randomly generated networks. We generate networks of 20 patches, where patch size ratios were either all the same 1:1 with $\theta = 0.001$ (circles), θ ratio 1:5 ($\theta_{larger} = 0.001$ and $\theta_{smaller} = 0.005$, where half of the patches contain ∼55% of the individuals in the larger patches) (triangles) or 1:10 (where patch sizes gradually decrease up to ∼40% the size of the largest patches, with two patches of each size, $\theta_n = 0.001n$ for $n = 1 : 10$) (diamond). Small deviations from these percentages occur across transmission modes, reflecting the different infection dynamics arising in each case. For each network, we track the global infection prevalence after 10^3 time steps for all parasite transmission modes, while varying connectedness a of the patches: FD (a-c), DD (d-f), V (g-i), FD+V (j-l), DD+V (m-o). Calculations were repeated for five different randomly generated networks and for three different combinations of dispersal propensities: (left column) $m_U = 0.25$ and $m_I = 75$; (middle column) $m_U = m_I = 0.5$; (right column) $m_U = 0.75$ and $m_I = 25$. All transmission modes are applied to each network. Population is initialized with $I_1 = 1$, $U_1 = 199$, for one patch and $I_n = 0$, $U_n = 200$ in all other patches. Other parameters: $\alpha_U = 1.04$, $\alpha_I = 0.98$, $d_U = 0.001$, $d_I = 0.002$, $\beta_h = 0.9$, $\beta_v = 0.9$, $c_{FD} = 2$, $c_{DD} = 0.02$, $\mu = 0.002$.

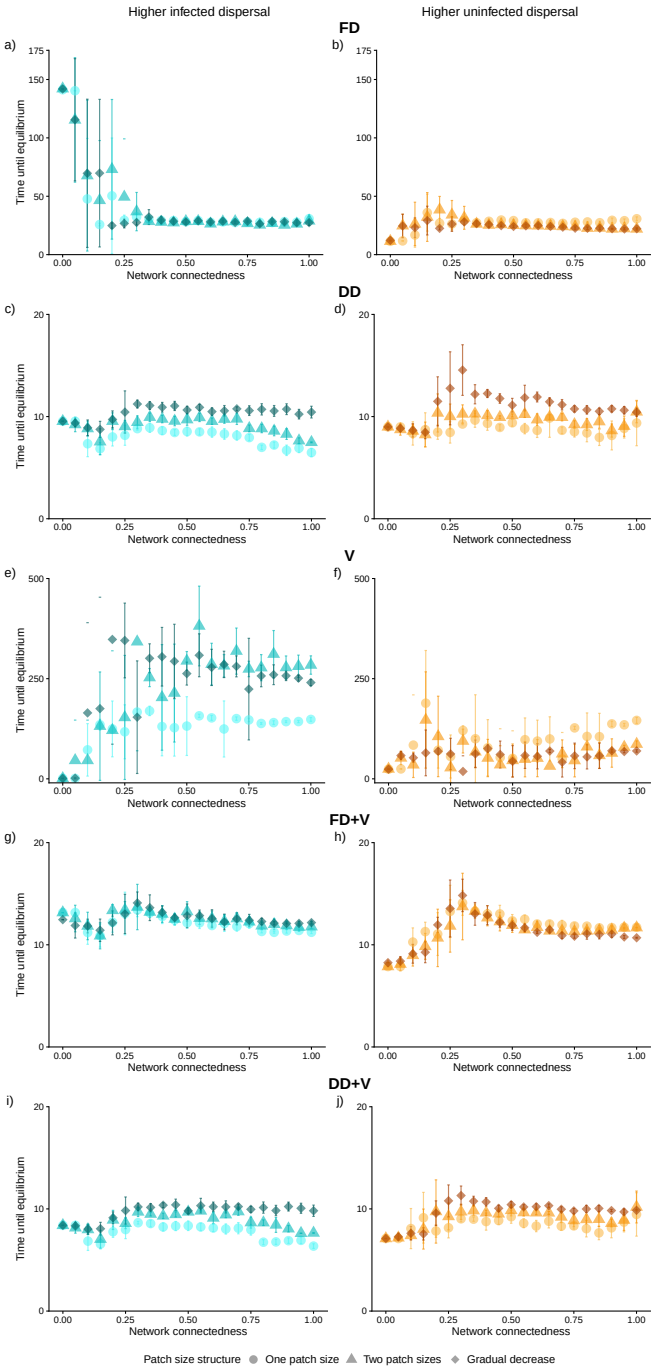

Fig. S12 Impact of transmission mode on time until equilibrium in randomly generated networks. We generate networks of 20 patches, where patch size ratios were either all the same 1:1 with $\theta = 0.001$, θ ratio 1:5 ($\theta_{larger} = 0.001$ and $\theta_{smaller} = 0.005$, where half of the patches contain ∼55% of the individuals in the larger patches) (triangles) or 1:10 (where patch sizes gradually decrease up to ∼40% the size of the largest patches, with two patches of each size, $\theta_n = 0.001n$ for $n = 1 : 10$) (diamond). Small deviations from these percentages occur across transmission modes, reflecting the different infection dynamics arising in each case. For each network, we track the global infection prevalence after 10^3 time steps for all parasite transmission modes, while varying connectedness a of the patches. We record the time to equilibrium frequency, defined as the time point at which changes in global infection frequency fall below a threshold of 10^{-17}. Calculations were repeated for five different randomly generated networks and for two different combination of dispersal propensities: (a,c,e,g,i) $m_I = 75$ and $m_U = 0.25$; (b,d,f,h,j) $m_I = 25$ and $m_U = 0.75$. All transmission modes are run with to each network. Other parameters: $\alpha_U = 1.04$, $\alpha_I = 1.3$, $d_U = 0.001$, $d_I = 0.002$ $\beta_h = 0.9$, $\beta_v = 0.9$, $c_{FD} = 2$, $c_{DD} = 0.02$, $\mu = 0.002$. Population is initialized with $I_1 = 1$, $U_1 = 199$, for one patch and $I_n = 0$, $U_n = 200$ in all other patches.